VOLUME 21, 1959/60, No. 1 pp. 1-40 Published 11th December 1959

Philips Technical Review

DEALING WITH TECHNICAL PROBLEMS
RELATING TO THE PRODUCTS, PROCESSES AND INVESTIGATIONS OF
THE PHILIPS INDUSTRIES

A RANGE OF PULSED MAGNETRONS FOR CENTIMETRE AND MILLIMETRE WAVES

by J. VERWEEL and G. H. PLANTINGA. 621.385.64.029.64:621.3.032.2

During the war years great strides were made in the development of the magnetron. Power outputs were raised from a few score watts to hundreds of kilowatts, and operating wavelengths reduced from some 20 cm to 1 cm. Progress since then has perhaps been less spectacular, but the following article, which describes a range of magnetrons for wavelengths of 32, 12, 8 and 4 mm, shows that advances are still being made in this field.

Introduction

In recent times the development of the magnetron has been mainly directed along the following lines [1]):

1) The achievement of higher pulse powers.
2) The attainment of shorter operating wavelengths.
3) The incorporation of tuning, i.e. increase of the frequency range.
4) The attainment of high continuous power outputs with high efficiencies.

Points 1) and 2) chiefly concern magnetrons for radar. With a shorter wavelength and the same size of aerial the received fraction of the transmitted power is greater and the beam narrower. This makes for better resolution of the image on the radar screen and allows the shape of objects to be better distinguished, which is important for short-range radar as used on airfields and in harbours. A radar installation of this kind equipped with an 8 mm magnetron will be the subject of a forthcoming article in this Review.

Point 4) may be of importance in shortwave therapy and also in electronic cookers, in which food is cooked or heated in a very short time by high-frequency radiation, usually of about 12 cm wavelength. Both applications are based on the high dielectric losses occurring in water at these wavelengths.

In this article attention will be devoted solely to points 1) and 2). We shall describe a range of experimental magnetrons designed at the Philips Research Laboratories, Eindhoven, for operation at wavelengths of about 32, 12, 8 and 4 mm. The peak power output of these tubes is, in round figures, respectively 1100, 70, 80 and 40 kW. In the case of the 32 mm magnetron the emphasis is placed on obtaining a high mean power as well as a high peak power. The other magnetrons may be regarded as steps on the way towards the highest possible operating frequency. All tubes are equipped with an L-type (dispenser) cathode, which has been found to give good results in magnetrons. The four tubes in question, together with some of their component parts, are shown in *fig. 1*, from left to right in order of diminishing wavelength.

Fig. 2 shows, from left to right, the 12 mm, 8 mm and 4 mm magnetrons each mounted in its permanent magnet. (No special magnet was developed for the 32 mm magnetron.)

In the design of magnetrons for ever higher frequencies, use can be made of the laws of similarity. This design technique will be discussed below. We shall then deal with the construction of the various tubes and with the engineering problems involved, and finally we shall compare the operating characteristics one with the other and in relation to the scaling laws derived from the similarity considerations.

[1]) For an introduction to the principles of magnetrons, see e.g. J. Verweel, Philips tech. Rev. **14**, 44-58, 1952/53. For a comprehensive treatment see G. B. Collins, Microwave magnetrons, Radiation Laboratory Series No. 6, McGraw-Hill, New York 1948.

Similarity considerations applied to magnetron design

The calculation of the parameters of a magnetron intended to meet specified requirements is in general so complex as to be virtually impracticable. For given dimensions and wavelength the theory (see [1])) postulates a minimum condition for the magnetic field B and also an approximately linear relation between B and the anode voltage V_a. Design follows primarily from experience and from analysis of existing magnetrons. The measured characteristics of a series of experimental magnetrons can then be used for making modifications until an optimum definitive design is evolved.

Another and more direct means of arriving at a new design, especially where it is the wavelength that is to be changed, is based on considerations of similarity. Suppose that a given magnetron at a given anode current I_a and anode voltage V_a requires a magnetic field B at which it delivers a certain power output with a wavelength λ. If we now scale up an existing magnetron so that its linear dimensions all become p times larger, then at the same current and voltage this magnetron will produce the same power output at the wavelength $p\lambda$, and for this it will require a magnetic field of strength B/p. If the similarity is exact, the specific conductance at a given position in the new magnetron should be $1/p$ times the specific conductance at the corresponding position in the old magnetron, and the same should apply to the electric field strength at the cathode.

The scaling laws appropriate to the various parameters of a magnetron can be deduced as follows. The charges, currents and fields in a magnetron can be found theoretically with the aid of Maxwell's equations (for the vacuum and the conductors) and the equations of motion for an electron:

$$\left.\begin{aligned} \operatorname{curl}\frac{\mathbf{B}}{\mu_0} &= \mathbf{S} + \varepsilon_0\frac{\partial \mathbf{E}}{\partial t} \\ \operatorname{curl}\mathbf{E} &= -\frac{\partial \mathbf{B}}{\partial t} \\ \operatorname{div}\mathbf{E} &= \varrho/\varepsilon_0 \\ \operatorname{div}\mathbf{B} &= 0 \\ m\frac{\mathrm{d}\mathbf{v}}{\mathrm{d}t} &= e\mathbf{E} + e[\mathbf{v}\times\mathbf{B}] \\ \mathbf{S} &= \sigma\mathbf{E} \text{ in the conductors} \\ \mathbf{S} &= \varrho\mathbf{v} \text{ in the vacuum,} \end{aligned}\right\} \quad \ldots\ldots (1)$$

where $\mathbf{E}$ is the electric field strength, $\mathbf{B}$ the magnetic induction, $\mathbf{S}$ the current density, ϱ the charge density, $\mathbf{v}$ the velocity of an electron (charge e, mass m) and σ the electrode conductivity ($\mu_0 = 4\pi\times10^{-7}$ H/m and $\varepsilon_0 = 10^{-9}/36\pi$ F/m). The boundary conditions are given by the geometry and the conductance of the electrodes, the anode voltage and anode current, the constant axial magnetic field and the electric field at the cathode.

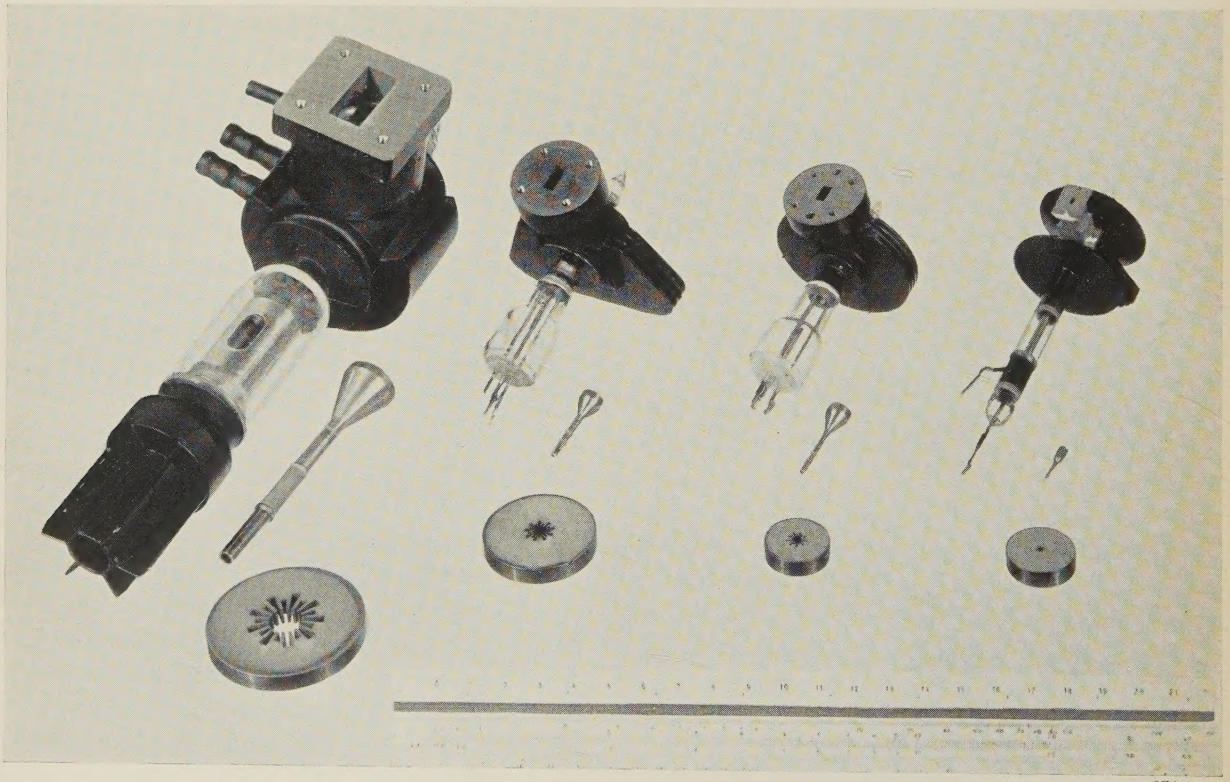

97418

Fig. 1. The four magnetrons discussed here for wavelengths of (from left to right) about 32, 12, 8 and 4 mm. Also depicted are the copper anode blocks (not yet machined to the correct diameter and height), and the cathode assemblies.

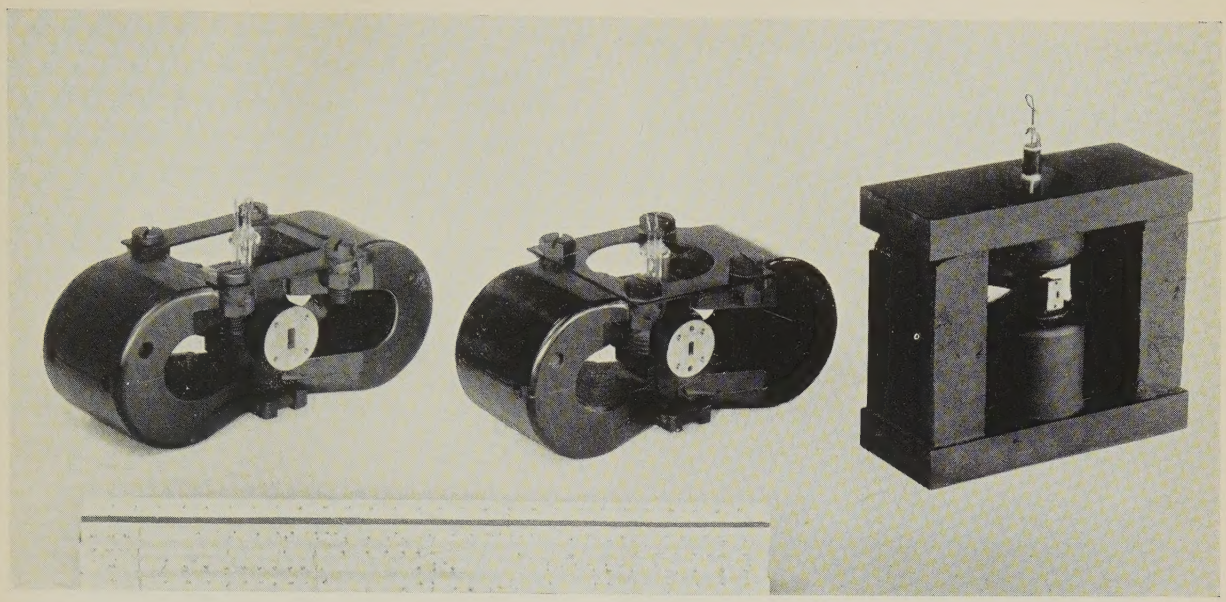

97419

Fig. 2. Left to right: the 12, 8 and 4 mm magnetrons mounted in their permanent magnets.

We consider two magnetrons *1* and *2*; all the dimensions of *2* are larger than those of *1* by a factor p. Taking a coordinate system (x_1, y_1, z_1) for *1* and a coordinate system (x_2, y_2, z_2) for *2*, both with their origin in the centre of the magnetron, we can define corresponding points by:

$$x_2 = px_1, \qquad y_2 = py_1, \qquad z_2 = pz_1 .$$

We define moreover as corresponding times:

$$t_2 = pt_1 .$$

Let all electromagnetic quantities of *1* be known; we give these the suffix 1. If we give these quantities in magnetron *2* the suffix 2, and we write, for corresponding positions,

$$\mathbf{E}_2 = \frac{\mathbf{E}_1}{p}; \qquad \mathbf{B}_2 = \frac{\mathbf{B}_1}{p}; \qquad \mathbf{S}_2 = \frac{\mathbf{S}_1}{p^2};$$

$$\varrho_2 = \frac{\varrho_1}{p^2}; \qquad \mathbf{v}_2 = \mathbf{v}_1; \qquad \sigma_2 = \frac{\sigma_1}{p},$$

all these quantities then satisfy equations (1) for the magnetron *2*. This is indeed evident from the fact that the operators curl and div are combinations of first derivatives with respect to the coordinates. For example, the component

$$\frac{\partial \mathbf{B}_2}{\partial x_2} = \frac{\partial (\mathbf{B}_1/p)}{\partial p x_1} = \frac{1}{p^2}\frac{\partial \mathbf{B}_1}{\partial x_1}, \quad \text{etc.}$$

It is found that the potentials, the currents and the Poynting vector are the same in both magnetrons.

For the given boundary conditions the quantities with suffix 2 thus constitute the solution for magnetron *2*, the power output being the same. Since corresponding times in magnetron *2*, as defined above, are p times longer than in magnetron *1*, the frequency of the oscillations generated by *2* is $1/p$ times that of *1*.

The various scaling laws should thus enable us, if we have for example an existing 3 cm magnetron for the required power output, to construct a 6 mm magnetron by reducing all dimensions five times and by increasing the magnetic field five-fold. The application of similarity principles, however, can encounter difficulties, such as the following.

1) Towards higher frequencies it is not, in general, possible to increase the electrode conductance correspondingly, for with increasing frequency the effective conductivity in fact decreases as a result of skin effect. The question then arises in how far the real situation can be described by attributing an infinitely high conductance to the anode block of both magnetrons — in which case the scaling law would again be satisfied. As regards the effect on the electric field pattern, which determines the electron motion, the resistance of the conductors can normally be disregarded. Obviously, however, this is not so as regards the energy losses due to the high-frequency currents in the tube walls: in the smaller magnetron a larger proportion of the high-frequency power supplied by the electron beam will be needed to maintain the oscillations in the tube. We shall return to this matter when comparing the results.

2) The scaling factor for the magnetic induction is that it should increase proportionately with the frequency. This causes no difficulty while the magnetic induction is substantially lower than the saturation induction of magnetic materials, since the magnetic air-gap is also reduced. The length of the required magnetic material then remains approximately the same. However, if the induction required approaches the saturation value, prohibitive difficulties arise in the design of the magnet.

3) Since, under conditions of similarity, the current remains unchanged, the current density must increase as the square of the frequency. It may then happen that the cathode emission in the original

magnetron is limited by the space charge, whereas in the scaled-down magnetron the emission is saturated (and possibly supplemented by secondary emission to bring it to the required value; this will be touched on presently). The electric fields at the cathode may not be related in the two cases exactly as given by the relevant scaling factor, i.e. strict similarity no longer exists. With further reductions in size a limiting cathode current will be reached which will call for modifications to the design.

4) Upon scaling-down, the voltage remains unchanged, which means that the electric field strength increases. It is therefore necessary to take into account the danger of electrical breakdown.

5) The requirements with respect to mechanical strength and dimensional tolerances can lead to difficulties in the construction of a scaled-down model.

6) The power output remaining unchanged, the dissipation per unit surface rises sharply upon scaling-down. In certain cases this will call for a more elaborate cooling system. With pulsed magnetrons there is always the additional possibility of reducing the *mean* power by using shorter pulses or a lower pulse-repetition frequency.

The foregoing shows that in order to produce an appropriate design it will sometimes be necessary for certain dimensions to differ from those found by scaling-down an existing tube. Examples will be encountered in the following pages.

General construction and some engineering details

The construction will be explained with reference to the cutaway 32 mm magnetron shown in *fig. 3*. The central part is the anode block *a*; the other components project from this along two mutually perpendicular axes.

The anode block is made from a solid copper cylinder, in which nine small and nine large resonant cavities are pressed in the form of sectors (constituting a so-called "rising sun" pattern) by means of a steel hob; the operation is known as hobbing [2]). The eighteen resonant cavities are coupled together primarily via the space between cathode and anode, and together form a resonator system having a series of natural frequencies. In practice the mode of oscillation used is that in which adjacent resonant cavities oscillate in anti-phase ("π mode"); the frequency of this mode is governed by the various dimensions. After hobbing, cylindrical recesses are machined to receive the other components. The first of these components are the two iron end pieces *b* and *c*, which function as pole pieces for the magnet; they fit in the anode block with a small clearance from the ends of the resonant cavities in order to minimize the air-gap for the axial magnetic field. The end pieces are provided with holes through which the cathode is inserted, and also with rings *d* and *e* of fernico, an alloy to which hard glass can be sealed. The glass ring sealed to *d* serves as insulation

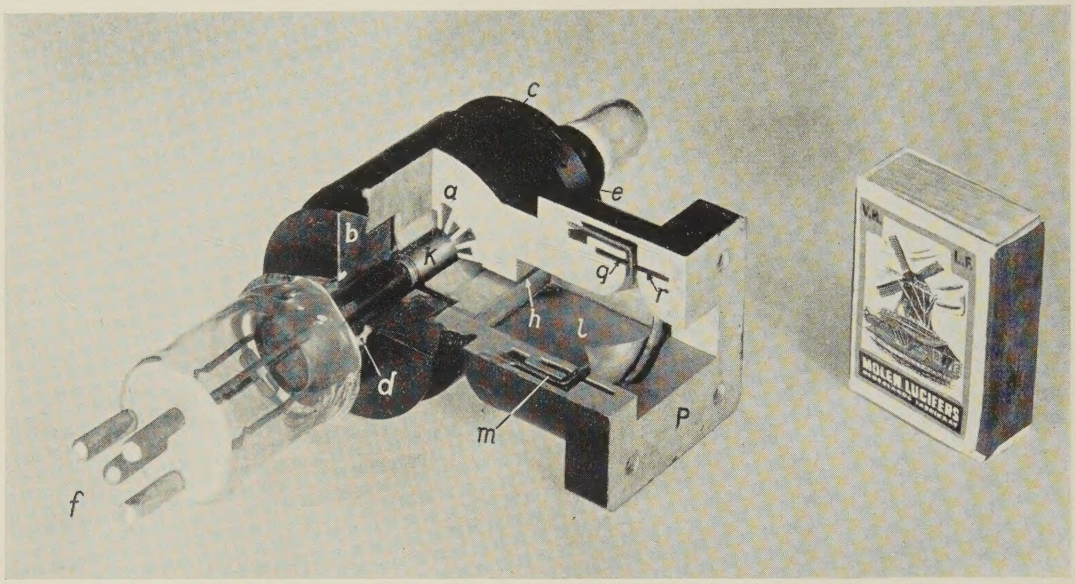

97420

Fig. 3. Cutaway view of 32 mm magnetron showing the following components: *a* anode block; *b* and *c* iron end pieces, serving as pole pieces; *d* and *e* fernico rings for hard-glass seals; *k* cathode; *f* connections for cathode and filament (as in fig. 4*a*); *h* transformer slot in copper disc; *l* output waveguide; *m* fernico cap with hole for glass output window; *p* brass connection flange; *q* and *r* slots functioning as RF chokes.

[2]) For further particulars of this process, see G. B. Collins, loc. cit., p. 654-661.

between cathode and anode, and the glass tube sealed to *e* forms the pinch via which the tube is exhausted.

The cathode *k* is an L-type or dispenser cathode, in the form of a porous tungsten cylinder of the same length as the anode block. End shields at the end of this cathode cylinder prevent the axial loss of electrons to the end shields, which would adversely affect the operation of the magnetron. The coiled filament inside the cathode cylinder is fed via the lead-ins through the glass at *f*.

Perpendicular to the axis of cathode and pole pieces is mounted the output system. For this purpose a recess is milled into the anode block so as to remove the rear wall of one of the resonant cavities. Against this a copper disc is fitted provided with a transformer slot *h* which couples the resonant cavity with the waveguide *l*. At the other end of *l* is a vacuum seal consisting of a round window sealed into the fernico cap *m*. (The window is absent in fig. 3.) Finally, the brass flange *p* enables *l* to be joined to the waveguide carrying the energy to the external circuit.

By means of the transformer slot *h* it is possible to adjust the load which the antenna constitutes on the anode system. When the load increases the magnetron efficiency increases also, but at a certain critical load the operation becomes unstable. Moreover, variations in the antenna impedance, such as arise with a rotating antenna, cause changes in the oscillating frequency which are greater the higher the load. It is usually required that, at a reflexion coefficient of 0.2, the maximum frequency drift, termed the pulling figure, should not exceed a specified value. This may involve some compromise in the efficiency. The necessary dimensions of the transformer slot can be determined partly by calculation and partly by experiment.

The window should be made of a type of glass with sufficiently low high-frequency losses, so that there is no danger of it melting at the specified frequency and the specified mean power. Where the mean power is particularly high, intensified air-cooling can be employed. In fig. 3 it can be seen that the waveguide is chamfered where the window fits; this reduces the heat development per cm^2 surface of window. The larger area of window also diminishes the risk of flash-over due to the high RF field strengths, which could easily damage the window. The cylindrical slots *q* and *r* in parts *l* and *p* serve to prevent energy leaking away along the window and the fernico cap; at this frequency they act as RF chokes.

The tube is assembled as follows. The various metal parts are brazed together, the required temperature being produced by high-frequency heating. This is done in a reducing atmosphere, so that the parts remain perfectly clean. After brazing, the glass-to-fernico seals are made and the tube, still without the cathode, is exhausted and tested for leaks. If this test proves satisfactory, the tube is opened up again and the cathode sealed in, special jigs being used to ensure true alignment. The tube is then finally exhausted and degassed, after which the cathode is activated. After sealing-off, the cooling jacket is fitted (not shown in fig. 3) and the coupling flange *p* secured to the assembly with tin solder. The magnetron can then be mounted between the pole pieces of a suitable magnet.

Some constructional details

The foregoing remarks apply equally to all four tubes of the range described. We shall now discuss some special problems that arise in the construction of the individual magnetrons.

High power

With the 32 mm magnetron the aim was to increase both the peak output power and the mean power. A peak power of about 1100 kW was achieved at a mean power of 900 W. The peak power increases with the anode current and the anode voltage; this also entails an increase in the requisite magnetic field. The theoretical limits of current and voltage are difficult to specify; in practice it is found that every magnetron finally becomes unstable as the current and voltage are increased and refuses to oscillate with reasonable efficiency. The maximum peak power is dependent, among other things, on the dimensions of the large and small resonant cavities, the most favourable values for which must be found empirically.

A high mean power calls primarily for good dissipation of the power losses. In the 32 mm magnetron the losses are of the same order of magnitude as the useful power and are dissipated in the anode, the cathode and the output window. The copper anode readily conducts the heat outside, and the use of water cooling permits the dissipation here of several hundreds of watts. If no special precautions are taken, the output window will break down at a useful power of about 500 W, when a few watts are dissipated in the glass. The window can be adequately cooled by passing a stream of air over it as mentioned above.

Dissipation in the cathode causes the greatest difficulty. This is due to back bombardment from those electrons in the interaction space that absorb

energy from the high-frequency field. Provided this dissipation is smaller than the heater power required for the cathode, the cathode temperature can be kept constant by reducing the heater current. However, if the back-bombardment power rises above the normal heater power, the cathode, even with zero heater current, becomes overheated, as a result of which the materials used deteriorate more quickly and the life of the cathode is curtailed. In the case of the 32 mm magnetron, several measures were adopted to keep the cathode temperature within reasonable bounds. In the first place the length of the emissive part (and hence the anode length) was made as large as possible without causing undesired resonance modes in the anode system. A longer system means a smaller cathode dissipation per cm^2. Furthermore the heat dissipation of the cathode was made as high as possible — just the opposite to what is done for the cathodes in other tubes. The rate of heat loss can be increased in the first place by improving the heat conduction. For this purpose thicker and better-conducting materials can be used for the cathode support and leads. Secondly one can attempt to increase the heat loss by radiation, which is considerable at the hottest part of the cathode surface. With the cathode in question this was done by giving the porous tungsten cylinder the roughest possible surface. *Fig. 4* shows side by side a cathode (*a*) for which no special measures have been taken to improve the heat dissipation, and a cathode (*b*) designed to give maximum heat dissipation. At an emitting-surface temperature of 1200 °C the heat dissipation was found to be 90 W at cathode *a* and 120 W at cathode *b*. The latter is the normal cathode dissipation for this tube at a mean power of 900 W. With the given dimensions of the emitting surface this probably represents the maximum heat dissipation obtainable in this way.

At these high values of mean power the L cathode is clearly superior to the oxide cathode, in view of the higher temperature which the L cathode needs for normal emission. Moreover an L cathode is much better able than an oxide cathode to withstand temperatures higher than the normal operating temperature.

High frequencies

We shall now discuss some of the difficulties involved in the scaling-down of dimensions by taking as an illustration the smallest magnetron of the range, the 4 mm type. The anode aperture is 1.4 mm in diameter. Around it are grouped 18 resonant cavities, separated one from the other by copper vanes 0.14 mm thick — precision work, beside which the mechanism of many a wristwatch looks positively coarse. Obviously the grinding of the hob for such a miniature system is no easy matter. Without going into details it may be mentioned that one aspect of the utmost importance is to keep the machined

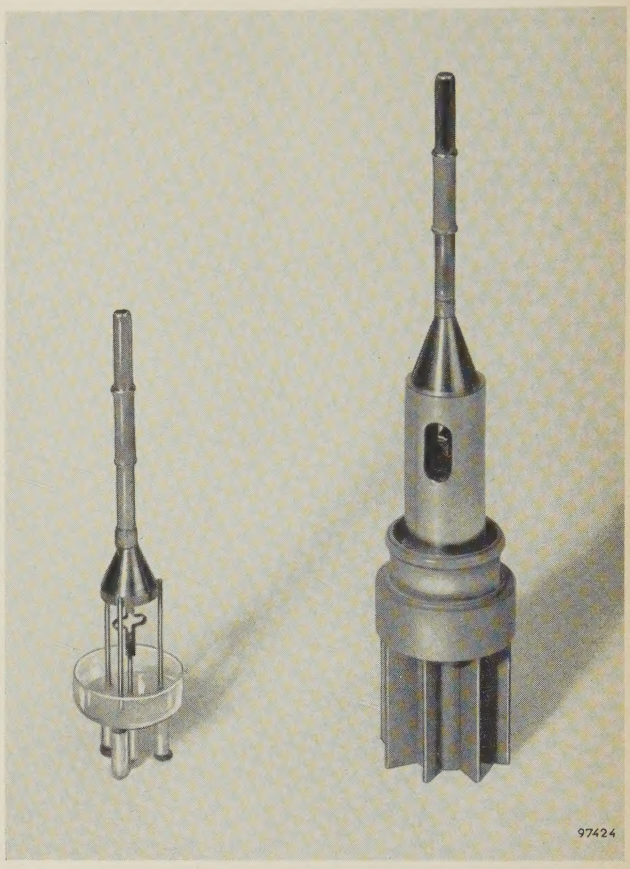

a *b*

Fig. 4. Cathodes for the 32 mm magnetron. Model *a* has a heat dissipation of 90 W, model *b* of 120 W.

metal, the support and the grinding tool at a constant temperature. A good hob is capable of making hundreds of anode systems.

The cathode, illustrated in *fig. 5*, has an emitting portion of 0.8 mm diameter. The greatest difficulty here was centring the cathode in the anode aperture, the distance between cathode and anode being only 0.3 mm. Although the cathode is very accurately sealed to the correct position by means of jigs, during the subsequent cooling the very slight deformation due to stresses in the glass and cathode components is still enough to cause impermissible eccentricity. This did in fact lead to many rejects. For this reason a special construction was adopted, as shown schematically in fig. 5. The anode block *a* with end pieces *b* and *c* is joined via the glass cylinder *d* to the cathode connection *e*. This part is assembled first, care being taken to align the hole of the collar

in *e* very accurately with the anode aperture. The cathode *k* is then introduced and centred in the anode system with the aid of a jig. This is made possible by a small clearance between the cathode and the collar in *e*. These parts are then soldered together at *g*. As a rule soldering causes much less deformation than the sealing process, and therefore good results can be obtained with this method. The final operation in this construction is to seal-in the filament pin *f*.

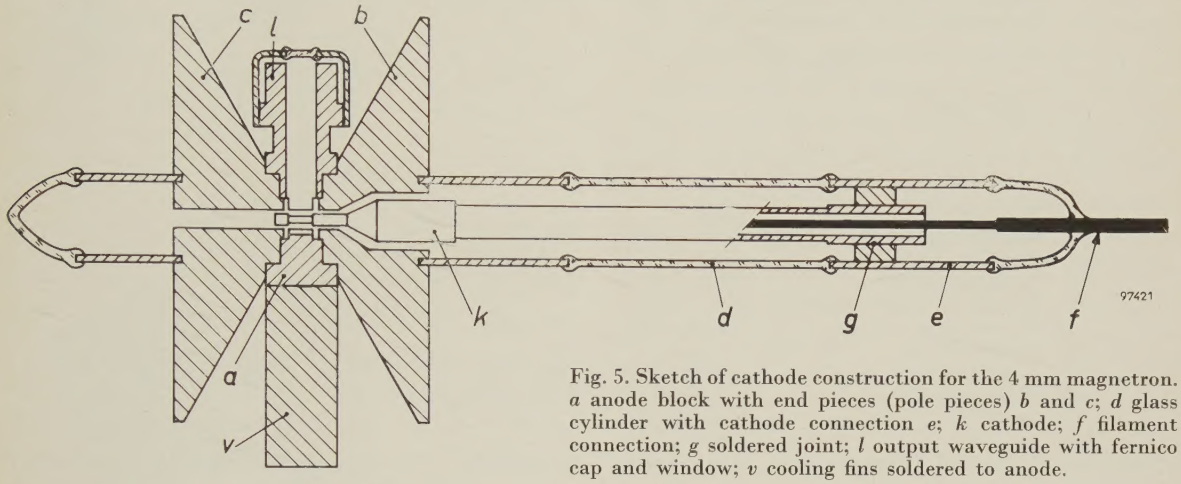

Fig. 5. Sketch of cathode construction for the 4 mm magnetron. *a* anode block with end pieces (pole pieces) *b* and *c*; *d* glass cylinder with cathode connection *e*; *k* cathode; *f* filament connection; *g* soldered joint; *l* output waveguide with fernico cap and window; *v* cooling fins soldered to anode.

The current density at the surface of the cathode in the 4 mm magnetron is about 200 A/cm². This is appreciably more than the saturation emission possible at reasonable cathode temperatures; the extra is supplied by the secondary emission due to back bombardment, which thus plays an essential role in this tube.

Comparison of results with the scaling factors derived from similarity considerations

The most important dimensions of a magnetron are denoted by letters in *fig. 6*. Column *a* in *Table I* gives the values of these dimensions and the exact wavelength in millimetres for each tube. To facilitate comparison, the dimensions are also expressed for each tube in terms of its wavelength (reduced dimensions, column *b*).

The table shows that, except for the anode length, the systems are in fact geometrically similar within narrow limits and that the measured wavelength is proportional to the linear dimensions. The reduced anode length in the 32 mm and 4 mm magnetrons is about twice that in the others. In the 32 mm magnetron this was done to obtain the highest possible mean power, the cathode dissipation per unit surface being — as we have seen — the chief limiting factor. In regard to the 4 mm magnetron the consideration was to obtain a high total operating current in spite of the limited emission current of the cathode. The advantage of changing the anode length in this connection is that, fundamentally, it has little effect on the operation, since, theoretically at least, no currents flow in the axial direction. (It is again the practical deviations from this that set a limit to the increase of this dimension.)

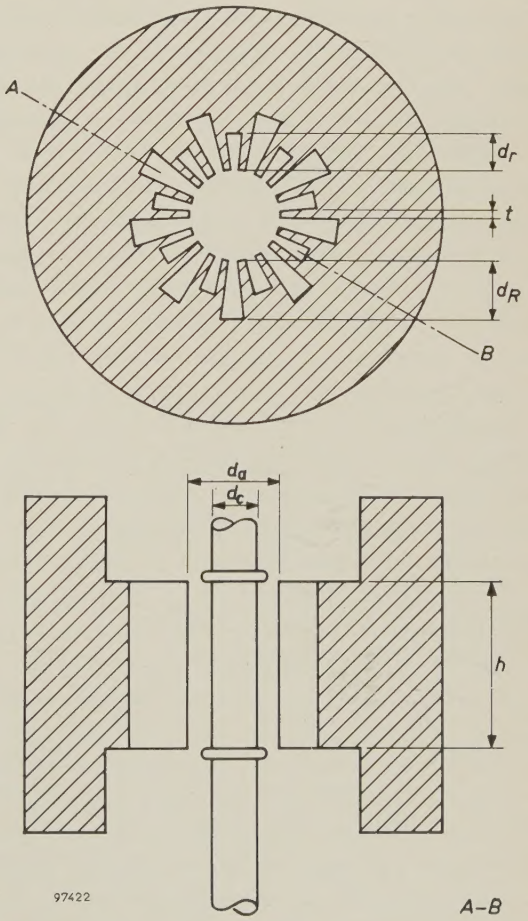

Fig. 6. Simplified cross-section of the magnetrons described here, indicating the principal dimensions: d_a = anode diameter, d_c = cathode diameter, h = anode length, d_r = depth of small resonant cavities, d_R = depth of large resonant cavities, and t = thickness of vane.

The principal characteristics of the magnetrons under discussion are represented in the performance charts in *fig. 7a, b, c* and *d*, in which contours of constant magnetic induction B, of constant power output P and of constant efficiency η are plotted with the anode current I_a and the anode voltage V_a as coordinates.

Table I. The principal dimensions (see fig. 6) of the four magnetrons, a in mm, b in terms of the wavelength as unit of length.

Dimension \ Magnetron	32 mm		12 mm		8 mm		4 mm	
	a	*b*	*a*	*b*	*a*	*b*	*a*	*b*
Wavelength λ	31.5		12.2		8.50		3.97	
Anode diameter d_a	10.6	0.34	4.05	0.33	2.90	0.34	1.40	0.35
Cathode diameter d_c	6.5	0.21	2.45	0.20	1.85	0.22	0.80	0.20
Anode length h	21.0	0.67	3.85	0.32	2.72	0.32	2.50	0.63
Depth of small resonant cavities d_r	4.10	0.13	1.59	0.13	1.16	0.14	0.56	0.14
Depth of large resonant cavities d_R	7.38	0.23	2.92	0.24	2.08	0.24	0.94	0.24
Thickness of vane t	1.12	0.036	0.43	0.035	0.308	0.036	0.143	0.036

Comparison of the charts for the four magnetrons reveals clearly the way in which a design according to the scaling law influences the characteristics. In general the maximum voltage and the maximum current are decreased by scaling-down, the first particularly because of the impossibility of generating sufficiently strong magnetic fields, and the second because of the limited emission current density of the cathode. To illustrate this the operating region of the 4 mm magnetron is shown shaded in all charts; strictly, the four performance charts can only be compared with each other in this region.

For a numerical comparison we may select two arbitrary points in the chart, namely those having the coordinates (6 A, 15 kV) and (4 A, 13 kV). If we consider these points for the 8 mm and 12 mm magnetrons, we see that, from similarity considerations, the corresponding points for the 32 mm and 4 mm magnetrons are those with twice the current, the anodes being relatively twice as long, i.e. the points (12 A, 15 kV) and (8 A, 13 kV), respectively. The values of the characteristics read from the charts at these points are given in *Table II*, together with the product $B\lambda$. In the η column we see that, with the exception of the 12 mm magnetron (see below), the efficiency decreases monotonically with the wavelength. This is due to the fact that the conductance decreases as the wavelength shortens (owing to skin effect), whereas the scaling factor requires it to increase. Measurements of the Q of the resonator system have shown that an efficiency drop of this order of magnitude is indeed to be expected.

The exception in the case of the 12 mm magnetron is due to the coupling to the waveguide being much looser, so that in this respect it is not a scaled-down model. As mentioned, this reduces efficiency, but its advantage is that it increases the stability, as appears from the pulling figure, which is here 16 Mc/s against 13 Mc/s with the 32 mm type and 32 Mc/s with the 8 mm type. (It will be recalled that the ratio of oscillating frequency to pulling figure is a measure of a magnetron's stability.)

The last column gives the product $B\lambda$ which, from similarity considerations, should remain unchanged when the dimensions are scaled-down. The table shows that this is true only to a first approximation. Singling out the 12 mm magnetron, we notice that this product decreases towards shorter wavelengths. The reason is to be found in the limited primary emission of the cathode; conditions of exact similarity do not therefore obtain with this range of magnetrons. In the 32 mm magnetron the saturation emission is not quite reached, and so the electric field at the cathode is virtually zero. The primary emission in the 4 mm magnetron, on the other hand, is saturated (see above), so that strong electric fields appear at the cathode. If, however, the cathode temperature in the 8 mm and 4 mm magnetrons is increased, the anode voltage and current

Table II. Comparison of characteristic values for the four magnetrons, read from the performance charts (fig. *7a, b, c, d*) at corresponding points according to similarity considerations. The comparison is made for two sets of points.

Wavelength λ (mm)	I_a (A)	V_a (kV)	B (Wb/m²)	P (kW)	η (%)	$B\lambda$ (10^{-4} Wb/m)
31.5	12	15	0.28	54	30	90
12.2	6	15	0.83	14	16	101
8.50	6	15	1.03	23	25	88
3.97	12	15	1.85	34	19	73
31.5	8	13	0.26	30	29	83
12.2	4	13	0.76	8	15	92
8.50	4	13	0.90	8	15	76
3.97	8	13	1.6	12.5	12	64

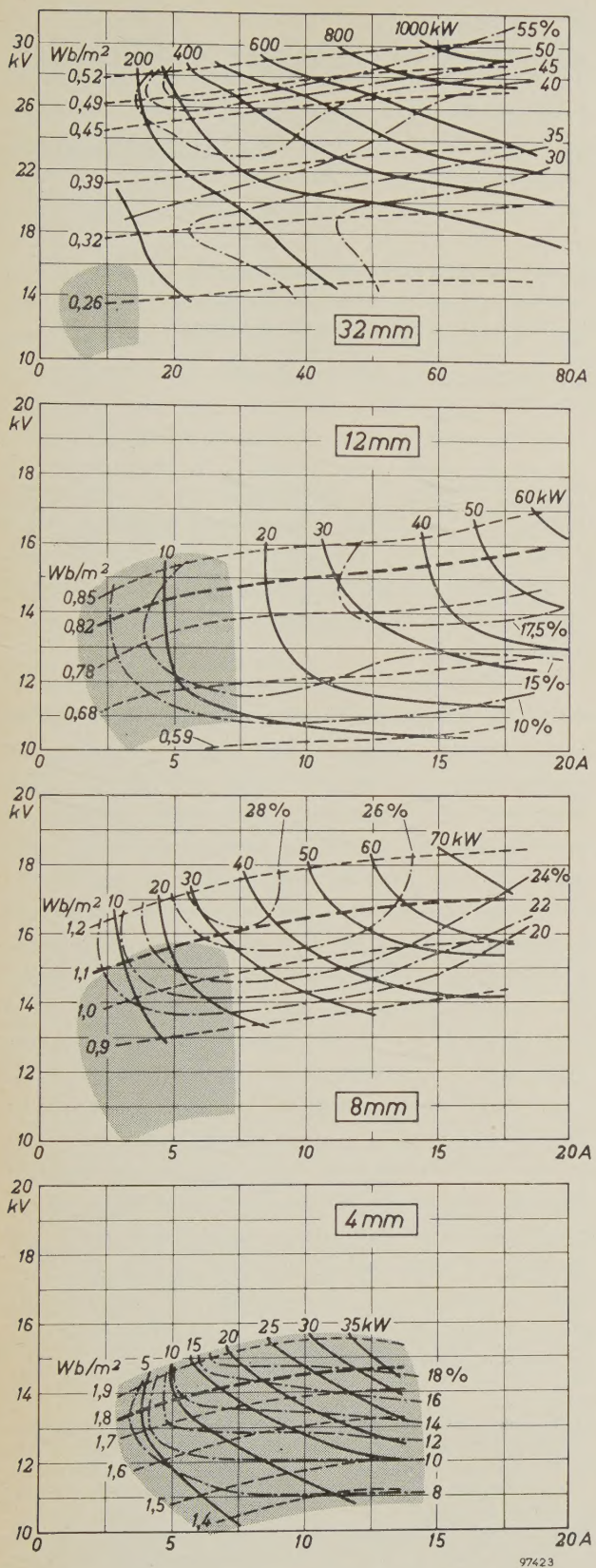

Fig. 7. Performance charts for the four magnetrons: *a*) 32 mm, *b*) 12 mm, *c*) 8 mm and *d*) 4 mm. On the abscissa the anode current I_a, on the ordinate the anode voltage V_a.
— — — — — Contours of constant magnetic induction B (the thicker contour in *b*, *c* and *d* relates to the field produced by the permanent magnet).
———— Contours of constant power P.
—·—·—·— Contours of constant efficiency η.

remaining the same, stronger magnetic fields are indeed required, i.e. the product $B\lambda$ is closer to the value expected from similarity considerations.

Life tests

The life tests on the magnetrons demonstrate the excellent properties of the L cathode. Not one of these tests was terminated by lowered emission. The most frequent cause of failure was leakage due to inadequate cooling; the 8 mm magnetron was still working well after a life test of almost 1500 hours. No life test has yet been made on the 4 mm magnetron. The results of the tests are given in *Table III*. The

Table III. Particulars of life tests on a 32 mm, a 12 mm and an 8 mm magnetron.

Wavelength in mm	31.3	12.2	8.35
Anode current in A	55	14	14
Anode voltage in kV	31	15.4	16.8
Peak power in kW at beginning of test	783	46	52
Peak power in kW at end of test	695	40	45
Efficiency in % at beginning of test	46	21	22
Efficiency in % at end of test	41	18	19
Pulse duration in μsec	2.0	0.44	0.50
Pulse-repetition frequency in c/s	500	2300	1000
Mean initial power in W	783	46	26
Duration of test in hours	238	700	1488

pulse durations and the repetition frequencies were rather arbitrarily chosen; the mean powers given for the 12 mm and 8 mm magnetrons are therefore not the maximum permissible values. A point of importance for short-range radar is that the 8 mm and 4 mm magnetrons work excellently with pulses of only 0.01 μsec.

Summary. An experimental range of magnetrons is described for wavelengths of 32, 12, 8 and 4 mm, and delivering peak outputs of 1100, 70, 80 and 40 kW, respectively. Since the four magnetrons have virtually the same geometrical proportions, the laws of similarity are theoretically applicable to them. It is found that the wavelength is proportional, and the requisite magnetic field inversely proportional, to the linear dimensions and that the same power is generated for the same anode voltage and current. Towards shorter wavelengths, however, difficulties arise owing *inter alia* to increasing high-frequency resistance, the limitation of the attainable magnetic field and cathode emission. Some constructional details are discussed. The "rising sun" anode system is hobbed from a solid copper block; to this are brazed iron end pieces (pole pieces). The coupling slot, the output waveguide and its glass window seal are also discussed. The axially mounted cathode is of the L type. Some special constructional problems are touched on with reference to the 32 mm and 4 mm magnetrons. The first was designed for a high mean power (900 W), which necessitated a cathode construction permitting a high rate of heat dissipation; the small dimensions of the 4 mm magnetron called for a special method of assembling the cathode in the tube. Comparison of the results of the various tubes shows that the wavelength is closely proportional to the linear dimensions and that the mutual disparities in efficiency can be satisfactorily explained. Life tests on a 32 mm, a 12 mm and an 8 mm magnetron were terminated after 238, 700 and 1488 hours, respectively; the power outputs had dropped in that time by about 15%.

THE RESISTANCE NETWORK, A SIMPLE AND ACCURATE AID TO THE SOLUTION OF POTENTIAL PROBLEMS

by J. C. FRANCKEN.

518.5:53.072.13:621.317.729

Among the methods that can be employed to solve the Laplace equation for given boundary conditions, that involving the use of a resistance network is in many cases highly attractive. It is a method applicable to two-dimensional problems and to three-dimensional problems where there is rotational symmetry. Setting-up the boundary conditions is particularly easy, the measurements do not take up much time, and remarkably accurate results are attainable.

In many branches of physics one is frequently confronted with potential problems, the solution of which involves finding a function φ which satisfies the Laplace equation, viz., in rectangular coordinates,

$$\frac{\partial^2\varphi}{\partial x^2}+\frac{\partial^2\varphi}{\partial y^2}+\frac{\partial^2\varphi}{\partial z^2}=0. \quad . \quad . \quad . \quad (1)$$

Examples of quantities satisfying the equation are the electrical potential in a space-charge free region and the gravitational potential in the space between the gravitating masses. The temperature under steady-state conditions of heat flow, and velocity potential in a non-turbulent stream of incompressible fluid are further examples. Usually the value of the potential function φ on certain closed surfaces, e.g. at solid boundaries, is known. In addition, sometimes the space in which φ must satisfy (1) is entirely enclosed by a surface at which φ is known. In other cases the space extends to infinity, at which φ approaches a known constant value. If φ represents temperature, the constant value will be the ambient temperature; if it represents electric potential, the constant value will be earth potential. The example we shall be using to illustrate the employment of the resistance network is drawn from electron optics, and concerns the potential distribution in electron guns for television picture-tubes. The surfaces where φ has known values will be those of the electrodes of the tube.

Only in a few simple cases is it possible to express the required potential function explicitly in terms of its given boundary values at certain surfaces. Usually one has to proceed by other methods. Apart from numerical methods, which are now widely employed in conjunction with digital computers, analogue techniques are particularly suited to potential problems. One well-known analogue technique involves the use of an electrolytic tank. A model of the electrode assembly, often an enlarged model, is submerged in a conducting liquid. The potential distribution existing when given voltages are applied to the electrodes is not altered when the model is submerged. The potential distribution in the electrolyte is measured with a probe [1][2][3]).

The electrolytic tank has proved to be a valuable aid in the solution of electron-optical problems. It has, however, its limitations and drawbacks: the construction of the electrode models is often laborious and expensive, and measurements in their vicinity are inaccurate because the liquid near the electrodes rises in consequence of capillarity. For three-dimensional problems with rotational symmetry tanks of "wedge" section are often used. A vertical section through this tank has the shape of a wedge. Electrodes can often be constructed from strips of metal, the disadvantages of complicated models thus being avoided. On the other hand a new disadvantage arises in that measurement near the axis of symmetry, precisely the most important region, is rendered very inaccurate by the marked capillary rise at the sloping bottom of the tank. It is not therefore surprising that, apart from the electrolytic tank, other analogue techniques have been developed for the purpose of determining potential distributions. One of these is the resistance network, which is the subject of the present article[4]).

---

[1]) G. Hepp, Measurements of potential by means of the electrolytic tank, Philips tech. Rev. **4**, 223-230, 1939.

[2]) N. Warmoltz, Potential distribution at the igniter of a relay valve with mercury cathode, Philips tech. Rev. **8**, 346-352, 1946.

[3]) An example of the use of the electrolytic tank for determining temperature distribution is described in F. Reiniger, The study of thermal conductivity problems by means of the electrolytic tank, Philips tech. Rev. **18**, 52-60, 1956/57.

[4]) Another method involves the use of conducting (graphite-surfaced) paper. This method can be employed for solving two-dimensional problems. Electrodes are simulated by cutting them out in copper foil. Conducting paper cannot be used for solving rotationally-symmetric three-dimensional problems, whereas the resistance network can be used in such cases.

In theory, the solutions it provides are only approximate; nevertheless in many cases these solutions are much more exact than those obtained with the aid of the tank. The resistance network was first proposed by Hogan [5]) and first used by De Packh [6]). However, the credit for pointing out the high degree of accuracy thereby attainable belongs to Liebmann [7])[8]).

Explanation of the principle of the network becomes more straightforward if the terms "differential operator" and "finite-difference operator" can be employed. We therefore start by giving a brief account of the two operators. Resistance networks for two-dimensional and for rotationally-symmetric three-dimensional problems are then discussed, followed by a description of an actual network of the latter kind, and of the manner in which it is used. This will be illustrated with the aid of a practical application. Finally, the implications of the fact that the network has finite meshes will be discussed with reference to two examples.

Differential and difference operators

The sum of the second differential coefficients with respect to x, y and z of any function $w(x,y,z)$ is often denoted by the symbol ∇^2:

$$\frac{\partial^2 w}{\partial x^2}+\frac{\partial^2 w}{\partial y^2}+\frac{\partial^2 w}{\partial z^2}\equiv \nabla^2 w. \quad . . \quad (2)$$

∇^2 is called the Laplacian operator. The effect of the operator on the function w will naturally depend on the point in space at which it is applied (i.e. $\nabla^2 w$ is again a function of x, y and z). We are now able to express the Laplace equation (i.e. (1) above) in words as follows: *a function satisfying the equation has the property that when operated on by the Laplacian* ∇^2, *the result is zero at every point.*

From the differential operator ∇^2 we shall now derive a finite-difference operator L that, operating on the same function at the same point, produces almost the same effect as ∇^2 itself, i.e. $Lw \approx \nabla^2 w$. For this purpose we consider an arbitrary point O and three pairs of points, P and Q, R and S, and T and U, which lie respectively in the x, y and z directions at a distance a on either side of O (*fig. 1*).

We can express the difference between the values w_Q and w_O of w at points Q and O by using Taylor's theorem. This gives us the difference in terms of a and the derivatives of w with respect to x at point O:

$$w_Q - w_O = a\left(\frac{\partial w}{\partial x}\right)_O + \frac{a^2}{2!}\left(\frac{\partial^2 w}{\partial x^2}\right)_O + \frac{a^3}{3!}\left(\frac{\partial^3 w}{\partial x^3}\right)_O + \frac{a^4}{4!}\left(\frac{\partial^4 w}{\partial x^4}\right)_O + \ldots . \quad (3a)$$

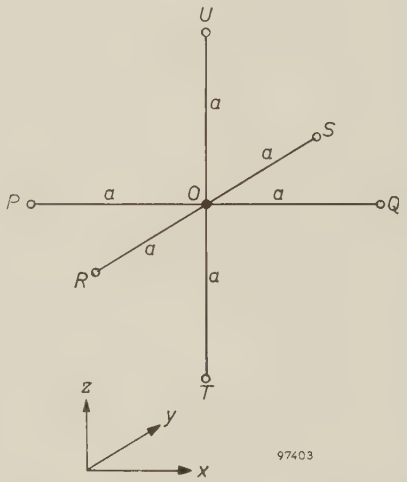

Fig. 1. Illustrating the derivation of the difference operator L.

By replacing a in the above by $-a$, we obtain a similar series for $w_P - w_O$:

$$w_P - w_O = -a\left(\frac{\partial w}{\partial x}\right)_O + \frac{a^2}{2!}\left(\frac{\partial^2 w}{\partial x^2}\right)_O - \frac{a^3}{3!}\left(\frac{\partial^3 w}{\partial x^3}\right)_O + \frac{a^4}{4!}\left(\frac{\partial^4 w}{\partial x^4}\right)_O - \ldots . \quad (3b)$$

Adding these two series and solving for $(\partial^2 w/\partial x^2)_O$, we obtain:

$$\left(\frac{\partial^2 w}{\partial x^2}\right)_O = \frac{1}{a^2}\{(w_Q - w_O) + (w_P - w_O)\} - \frac{a^2}{12}\left(\frac{\partial^4 w}{\partial x^4}\right)_O - \ldots . \quad (4)$$

The differential coefficient $(\partial^2 w/\partial x^2)_O$ is thus expressed in terms of the differences $(w_Q - w_O)$ and $(w_P - w_O)$ plus a number of correction terms, whose total value can be made as small as desired simply by making a small enough.

$(\partial^2 w/\partial y^2)_O$ and $(\partial^2 w/\partial z^2)_O$, the other differential coefficients occurring in (2) above, can be expressed as differences in an analogous manner. Inserting in (2) the expressions thus obtained, we have:

---

[5]) T. K. Hogan, A general experimental solution of Poisson's equation for two independent variables, J. Instn. Engrs. Austr. **15**, 89-92, 1943.

[6]) D. C. de Packh, A resistor network for the approximate solution of the Laplace equation, Rev. sci. Instr. **18**, 798-799, 1947.

[7]) G. Liebmann, Solution of partial differential equations with a resistance network analogue, Brit. J. appl. Phys. **1**, 92-103, 1950.

[8]) G. Liebmann, Field plotting and ray tracing in electron optics, Advances in electronics **2**, 101-149, 1950.

$$(\nabla^2 w)_O = \frac{1}{a^2}(w_P + w_Q + w_R + w_S + w_T + w_U - 6w_O) - \\ - \frac{a^2}{12}\left(\frac{\partial^4 w}{\partial x^4} + \frac{\partial^4 w}{\partial y^4} + \frac{\partial^4 w}{\partial z^4}\right)_O - \ldots \quad (5)$$

Introducing the operator L, we now put:

$$(Lw)_O = \frac{1}{a^2}(w_P + w_Q + w_R + w_S + w_T + w_U - 6w_O). \quad \ldots \quad (6)$$

We see from (5) that $(Lw)_O$ is an approximation to $(\nabla^2 w)_O$, approaching it all the more closely according as a is made smaller. L is the *finite-difference operator* referred to above; it is so called because L denotes an operation whereby the finite differences $w_P - w_O$, etc. are used.

This procedure for deriving a difference operator from a differential operator can also be followed in the more general case where the differential equation involves the first derivatives ($\partial w/\partial x$, etc.) as well as the second derivatives. By subtracting equations (3a) and (3b) from each other, one can arrive at an expression for $(\partial w/\partial x)_O$ involving $(w_P - w_O)$ and $(w_Q - w_O)$ and a series of correction terms whose sum approaches zero as a goes to zero. We shall make use of this when dealing with three-dimensional problems with rotational symmetry.

In the special case where w is independent of z, we have $w_T = w_U = w_O$, and (6) simplifies to

$$(Lw)_O = \frac{1}{a^2}(w_P + w_Q + w_R + w_S - 4w_O). \quad (7)$$

We can now go on to discuss the principle of the resistance network.

A resistance network for two-dimensional problems

To start with we shall confine ourselves to two-dimensional cases. There is then one direction — the z-direction say — in which the function being sought does not vary. In these cases $\partial^2\varphi/\partial z^2 = 0$, and Laplace's equation assumes the form:

$$\frac{\partial^2 \varphi}{\partial x^2} + \frac{\partial^2 \varphi}{\partial y^2} = 0. \quad \ldots \quad (8)$$

To take a definite case, let us consider the example shown in *fig. 2*. The three closed outlines s_1, s_2 and s_3 represent sections taken at right angles through three infinitely long prisms. On the periphery of each prism φ has a known constant value. The problem is to find a function φ which satisfies (8) in the area within s_3 but outside s_1 and s_2, and which assumes the prescribed values along s_1, s_2 and s_3.

Over s_1, s_2 and s_3 we place a square grid, the lines of which are parallel to the x and y axes and spaced at intervals of a (see fig. 2). The "grid lines" intersect at "grid points". We shall refer to two grid points as "adjacent" if their distance apart is the mesh width a. In fig. 2 the outlines s_1, s_2 and s_3 have been drawn in such a way that they intersect the grid only in grid points. This is not a necessary limitation, but it will simplify discussion, and the examples we shall be dealing with will subject to it.

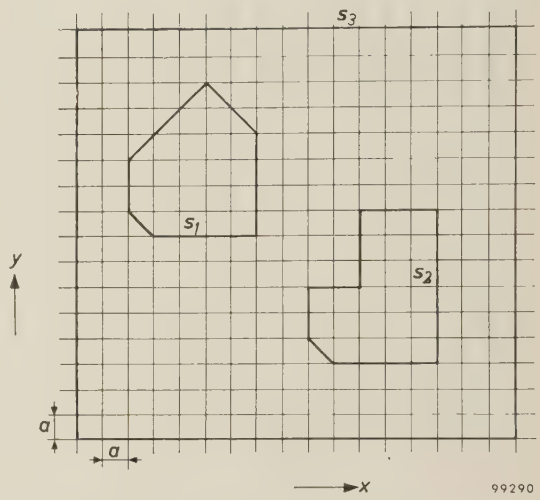

Fig. 2. The unknown function φ has known values along the outlines s_1, s_2 and s_3. Throughout the area inside s_3 but outside s_1 and s_2 it must satisfy the Laplace equation. It is assumed that s_1, s_2 and s_3 are such that they intersect a superposed square grid (mesh width a) only in grid points.

We shall refer to grid points located on the outlines s_1, s_2 and s_3 as "boundary grid points", and to the remaining ones in the area wherein φ has to be determined as "internal grid points".

The following proposition underlies the principle of the resistance network employed.

If each internal grid point is allotted a value φ^* such that between the value φ^* at any such point and the values at adjacent grid points the relationship $L\varphi^* = 0$ exists and if at the boundary grid points φ^* has the boundary values specified for the required function φ at those places, then the difference between φ^* and φ at the internal grid points will approach zero as the mesh width (a) approaches zero.

As we have already pointed out, there is a close connection between the difference operator L and the differential operator ∇^2; the proposition just stated is accordingly a plausible one. Its truth can be proved rigorously by demonstrating that at all grid points $\varphi - \varphi^*$ is smaller than a certain finite

quantity that approaches zero as the mesh width a does so [9]).

For the purpose of finding φ^* values, a network of resistors is built up. We shall see later what requirements the component resistors have to satisfy. The junctions of the resistance network will correspond to the grid points in fig. 2; accordingly, four resistors will meet at each junction (*fig. 3*). We shall refer to junctions corresponding to boundary grid points as "boundary junctions". Between the boundary junctions we may apply voltages that are proportional to the differences between φ values in the corresponding boundary grid points. If the lowest value of φ at any of the boundary grid points is $\varphi_{\min}$ and if we take the potential of the corresponding boundary junction as a datum for measuring the potentials V_b of other boundary junctions, then any of these latter potentials is given by

$$V_b = (\varphi_b - \varphi_{\min})/\beta. \quad . \quad . \quad . \quad . \quad . \quad (9)$$

The suffix b to V and φ indicates that they relate to *boundary* junctions in the resistance network and

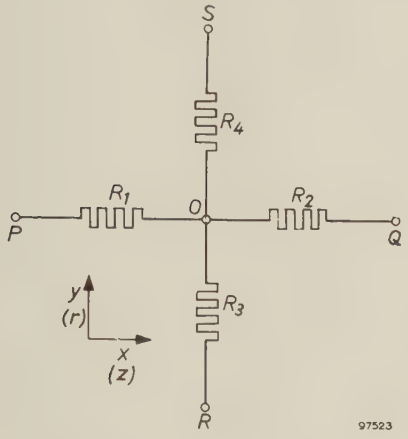

Fig. 3. Resistors R_1, R_2, R_3 and R_4 meet at O, a junction in the resistance network. In the two-dimensional case, PQ represents a line parallel to the x-axis, and RS a line parallel to the y-axis; in the rotationally-symmetric three-dimensional case PQ represents a line parallel to the z-axis, RS one parallel to the r-axis.

to the corresponding boundary grid points. $1/\beta$ is a constant of proportionality. We now allot to each *internal* grid point a value

$$\varphi^* = \beta V + \varphi_{\min}, \quad . \quad . \quad . \quad . \quad (10)$$

where V is the potential measured at the corresponding junction in the resistance network. Through a resistor connecting two adjacent junctions in the network, e.g. that between P and O in fig. 3, flows a current having the value $(V_P - V_O)/R_1$. Applying Kirchhoff's law to junction O, we find that

$$\frac{V_P - V_O}{R_1} + \frac{V_Q - V_O}{R_2} + \frac{V_R - V_O}{R_3} + \frac{V_S - V_O}{R_4} = 0.$$

From this and from (10) it follows that for any grid point O,

$$\frac{\varphi_P^* - \varphi_O^*}{R_1} + \frac{\varphi_Q^* - \varphi_O^*}{R_2} + \frac{\varphi_R^* - \varphi_O^*}{R_3} + \frac{\varphi_S^* - \varphi_O^*}{R_4} = 0. \quad . \quad (11)$$

Comparison of (11) with (7) makes it clear that, *if all four resistors have the same value*,

$$(L\varphi^*)_O = 0$$

at any grid point O. Since, in addition, φ^* on the boundary curves has the boundary values laid down for φ, φ^* constitutes an approximation to the required function φ, provided all resistors composing the network are of the same value. The question as to how close the approximation is will be dealt with at the end of the article.

Three-dimensional problems with rotational symmetry

More common than two-dimensional problems are three-dimensional problems with rotational symmetry. If the rectangular coordinates are converted to cylindrical coordinates (r, z and ϑ in *fig. 4*), the z-axis being made to coincide with the axis of symmetry, the Laplace equation assumes the form:

$$\frac{\partial^2\varphi}{\partial r^2} + \frac{1}{r}\frac{\partial\varphi}{\partial r} + \frac{\partial^2\varphi}{\partial z^2} = 0. \quad . \quad (12)$$

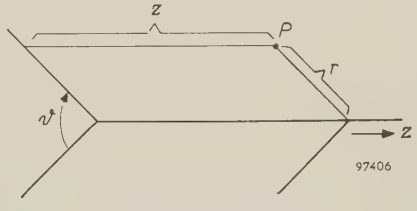

Fig. 4. r, z and ϑ, cylindrical polar coordinates of a point P.

[9]) See S. Gerschgorin, Z. angew. Math. Mech. **10**, 373-382, 1930, or L. Collatz, Numerische Behandlung von Differentialgleichungen, Springer, Berlin, 2nd edition, 1955, p. 320 et seq. Obtaining numerical solutions of the Laplace equation likewise often involves the solution (preferably with the aid of a computer) of the finite-difference equation $L\varphi^* = 0$, and the results obtained are accordingly only approximate. However, these methods can be based on difference operators that are better approximations to the Laplacian than L is, the series of correction terms in (5) beginning with a higher power of a than a^2. If terms involving a^2 etc. are to be eliminated, additional equations must of course be available; this means considering not only adjacent grid points, but also additional grid points in the vicinity of a given grid point. See for example Collatz, loc. cit., p. 352.

Owing to the rotational symmetry ϑ, does not appear in the equation. As in the two-dimensional case, therefore, we have a differential equation involving two independent variables, these being z and r instead of x and y. The Laplacian operator is now

$$\left(\frac{\partial^2}{\partial r^2}+\frac{1}{r}\frac{\partial}{\partial r}+\frac{\partial^2}{\partial z^2}\right). \quad . \quad . \quad . \quad . \quad (13)$$

In order to derive a finite-difference operator from (13), we let (13) operate on an arbitrary function $u(z,r)$, and consider a point O and the two pairs of points P,Q and R,S which lie in the z and r directions respectively, at a distance a on opposite sides of O. Expressing the differential coefficients as differences, in the same manner as on pp. 11 and 12, we arrive at the following:

$$\left(\frac{\partial^2 u}{\partial r^2}+\frac{1}{r}\frac{\partial u}{\partial r}+\frac{\partial^2 u}{\partial z^2}\right)_O = (\mathrm{M}u)_O - \\ -\frac{a^2}{12}\left(\frac{\partial^4 u}{\partial r^4}+\frac{2}{r}\frac{\partial^3 u}{\partial r^3}+\frac{\partial^4 u}{\partial z^4}\right)_O \quad \ldots, \quad . \quad . \quad . \quad (14)$$

where

$$(\mathrm{M}u)_O = \frac{1}{a^2}\Big\{(u_P-u_O)+(u_Q-u_O)+ \\ +\left(1-\frac{a}{2r}\right)(u_R-u_O)+\left(1+\frac{a}{2r}\right)(u_S-u_O)\Big\}. \quad (15)$$

The required finite-difference operator M is thus defined by (15).

We now superpose on the z,r-plane a square grid with a mesh width of a. The mathematical proposition stated for L on p. 12 is also valid for M [10]). The values of φ^* that are allotted to the internal grid points must now satisfy the relationship

$$\mathrm{M}\varphi^* = 0, \quad (16)$$

while φ^* at the boundary grid points must have the boundary values laid down for φ. φ^* will then be an approximation to φ; in other words, φ^* will approach φ as the mesh width a approaches zero.

As before, it is possible to build up a resistance network whose junctions have potentials corresponding to φ^* values. In order to deduce the requirements the resistors will have to satisfy, we shall proceed as before, but this time (11) must be compared with (15). Having done this, we find that φ^* satisfies the relationship $(\mathrm{M}\varphi^*)_O = 0$ provided that

$$\frac{1}{R_1}:\frac{1}{R_2}:\frac{1}{R_3}:\frac{1}{R_4} = 1:1:\left(1-\frac{a}{2r}\right):\left(1+\frac{a}{2r}\right) \quad (17)$$

(see fig. 3).

If the grid is so positioned that the z-axis coincides with one of the grid lines, then at each of the grid points

$$r = ja,$$

j being an integer. (17) now becomes:

$$\frac{1}{R_1}:\frac{1}{R_2}:\frac{1}{R_3}:\frac{1}{R_4} = 2j:2j:(2j-1):(2j+1). \quad (18)$$

In the present case, then, the resistance values must decrease with increasing distance from the z-axis. In the network shown in *fig. 5*, (18) is satisfied for all values of j except $j=0$. This exception is a point that we must look into.

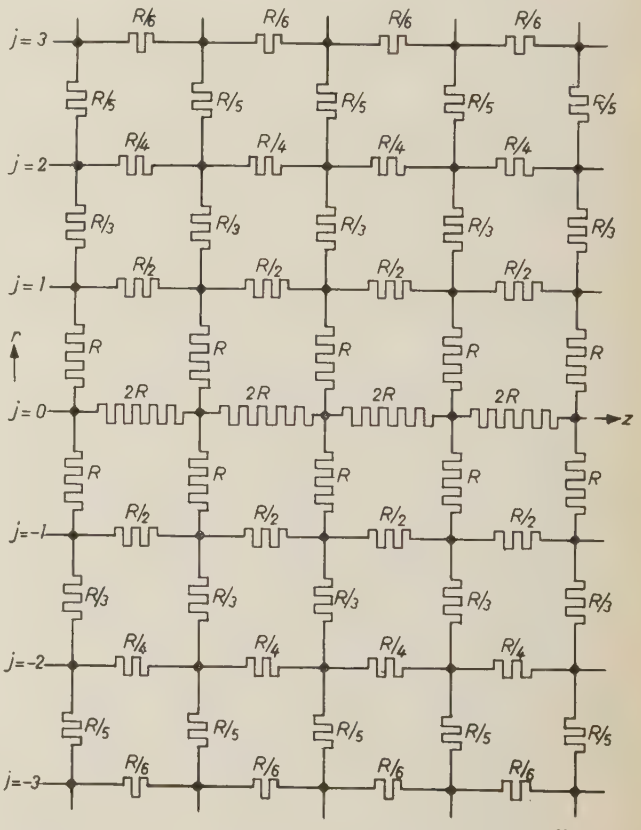

Fig. 5. Part of a network for rotationally-symmetric three-dimensional problems. Resistors meeting at junctions at which $j \neq 0$ have values satisfying the relation (18). For $j = 0$ (junctions on the axis) the resistors satisfy (20).

The resistors lying along the axis

The zero value of j, appropriate to points on the axis of symmetry (z-axis), gives rise to complications. This is clear for example from the conclusion

[10]) For the proof, see Gerschgorin, loc. cit. The proof given there is a general one valid for all elliptical differential equations. (8) and (12) are equations of this type.

that can be drawn from (18), namely that for resistors meeting at a junction on the axis, R_3 must be negative if R_1, R_2 and R_4 are positive. In addition, (14) and (15) involve indeterminate 0/0 terms when $r = 0$ [11]). These complications can be avoided by reverting to the finite-difference operator L (see (6)) as an approximation to the Laplace operator for points along the z-axis. The reason we abandoned L in favour of operator M when we took up the three-dimensional case with rotational symmetry was that the former would have led to a three-dimensional network. This objection does not, however, apply to points on the axis of symmetry. Let us consider a point O on that axis (see fig. 1; we shall assume that the x-axis in this figure represents the axis of symmetry). At point O, then,

$$w_T = w_R = w_U = w_S .$$

For such a point, therefore, we can rewrite (6) in the form

$$(\mathrm{L}w)_O = \frac{1}{a^2}\{(w_P - w_O) + (w_Q - w_O) + 2(w_R - w_O) + 2(w_S - w_O)\} . \quad . \quad . \quad (19)$$

Comparison of (11) with the above expression makes it clear that, in the grid points on the z-axis, φ^* will satisfy $\mathrm{L}\varphi^* = 0$ provided that

$$\frac{1}{R_1} : \frac{1}{R_2} : \frac{1}{R_3} : \frac{1}{R_4} = 1 : 1 : 2 : 2 . \quad . \quad (20)$$

These conditions have in fact been satisfied in the network of fig. 5, where the resistors forming the axis have the value $2R$.

The network of fig. 5 is not used in practice; practical versions extend to one side of the z-axis only. Such networks are perfectly satisfactory if the axial resistors are given a value of $4R$ instead of $2R$. The validity of this can be confirmed by reasoning as follows. Imagine the $2R$ resistance along the z-axis in fig. 5 to have been replaced by two $4R$ resistances in parallel, as in *fig. 6a*. On account of the rotational symmetry of the system, no current flows from the upper portion to the portion under the z-axis. The lower portion can therefore be omitted (fig. 6*b*) without making any difference to the upper portion [12]).

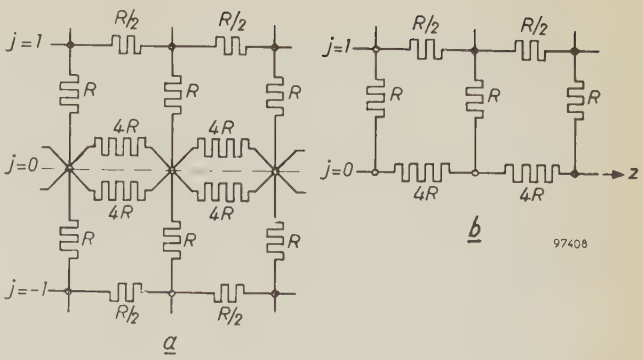

Fig. 6. Network (*a*) is equivalent to that in fig. 5, the $2R$ resistors along the z-axis having been replaced by two parallel $4R$ resistors. On account of symmetry, no current flows from the part of the network below the z-axis to the part above it. The lower half can therefore be removed without affecting the upper half, as in (*b*).

Design and use of the resistance network

Resistance networks suitable both for two-dimensional problems and for three-dimensional problems with rotational symmetry have been constructed in several Philips Laboratories. The two designs are identical apart from the values of the resistors and we shall therefore confine ourselves to describing the network for solving rotationally-symmetric three-dimensional problems. This network is constructed according to the arrangement shown in fig. 6*b*. It extends over 50 meshes in the z-direction and over 25 in the r-direction, and is accordingly composed of $(51\times25) + (26\times50) = 2575$ resistors in all, which are mounted on the back of a sheet of insulating material (*fig. 7*). The junctions have silver-plated contact pins that pass through to the front of the panel.

In order to determine the potential distribution in some electrode assembly (for example), the system is simulated on the resistance network by linking the junctions corresponding to the electrode outlines with copper wire. In principle it would be possible to apply voltages across the simulated electrodes in the manner described above (p. 13, first column). This is not necessary, however: by the

[11]) Along the axis, $\partial\varphi/\partial r$ and the other odd-order derivatives with respect to r are all zero in consequence of the symmetry of the system. Hence the middle term of differential operator (13) becomes 0/0; similar indeterminacies occur in the correction terms of (14). If the terms of the finite-difference operator (15) (with u replaced by φ) are arranged in a slightly different manner, the expression $(a/2r)(\varphi_Q - \varphi_P)$ appears which likewise has the value 0/0.

[12]) The network of fig. 6*b* can be arrived at directly by writing (19) in the form:

$$(\mathrm{L}w)_O = \frac{1}{a^2}\{(w_P - w_O) + (w_Q - w_O) + 4(w_S - w_O)\} .$$

On comparing (11) with the above, we obtain the condition

$$\frac{1}{R_1} : \frac{1}{R_2} : \frac{1}{R_3} : \frac{1}{R_4} = 1 : 1 : 0 : 4 ,$$

which is satisfied if $R_1 = R_2 = 4R$, $R_3 = \infty$ and $R_4 = R$.

Fig. 7. Some of the 2575 resistors composing the network designed for three-dimensional problems with rotational symmetry.

following simple procedure the required potential distribution can be found more conveniently. One of the electrodes, G for example (see *fig. 8*), is connected to terminal B of potentiometer AB, and all the other electrodes (K and A_1 in fig. 8) are connected to A, the other potentiometer terminal. A and B are connected up to an accumulator. To measure the potential at, say, the junction P, the latter is connected to the slide contact of the potentiometer via a null indicating instrument. Once the slide has been brought to a position where the null indicator shows a null reading, the potentiometer setting indicates the potential difference between P and A (or B) as a proportion of the potential difference between B and A. The value thus found is therefore the potential of P when electrode G has unit potential and all the other electrodes have zero potential. By repeating the measurements for the other junctions one obtains the potential distribution under the above-mentioned circumstances. One of the other electrodes, A_1 for example, is now given an effective potential of unity and the others are held at zero; the potential distribution is then measured again. The potential distribution for any given combination of electrode potentials is then found simply by combining these results linearly (superposition). Generalizing, if there are n electrodes instead of three, the measurements have to be repeated $n-1$ times in order to find, by linear combination of the results, a solution for any given set of electrode potentials. The convenience of this method lies in the fact that no adjustment or measurement of voltage is necessary.

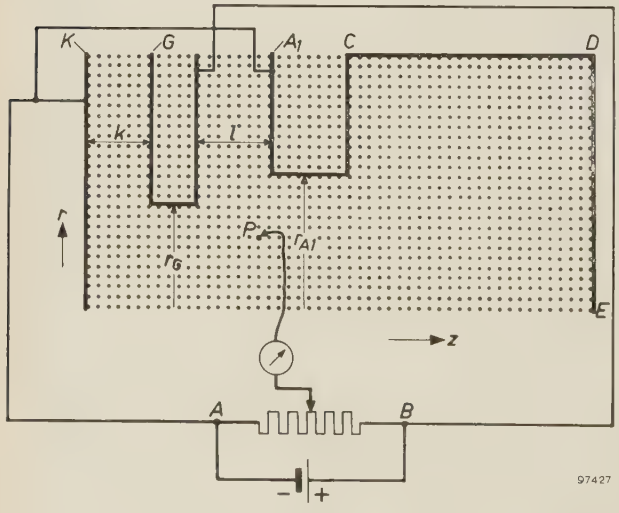

Fig. 8. Bridge circuit for measuring the potentials of junctions in the resistance network. K, G and A_1 are electrode models. The configuration is the same as in fig. 9. AB is a 1000 Ω potentiometer with a setting error of about 0.01 Ω. The null indicator is an electronic D.C. millivoltmeter with an internal resistance of 0.6 MΩ.

In view of the accuracy required, all the resistors were wound from manganin wire, to tolerances of $\pm 0.2\%$. Liebmann [7]) has pointed out that the average error arising in the measurement of potential, due to inexact resistance values, is much smaller than the errors in the resistances themselves, being from a tenth to a hundredth thereof. This is a consequence of the statistical properties of the network, whereby errors are levelled out. The temperature coefficient of manganin is so small, the voltage employed (usually about 2 V) is so low and the physical dimensions of the resistors are so large that there is no fear of errors due to heating-up of the resistors.

The upper limit to the (in principle, arbitrary) value of R (see fig. 6*b*) is fixed by the requirement that the highest value in the network, which is $4R$, shall not be an unreasonably high one for wire-wound resistors. On the other hand the smallest resistors must not have too low a value, otherwise the current through them would be large enough to set up appreciable potential differences in the copper wires representing the electrode outlines. In the present networks, R has the value 3600 Ω. The extreme resistance values are therefore $4R = 14\,400$ Ω and $R/50 = 72$ Ω.

A valve voltmeter type GM 6010 [13]) serves as the null indicator. It is a D.C. millivoltmeter combining

[13]) A. L. Biermasz and A. J. Michels, An electronic D.C. millivoltmeter, Philips tech. Rev. **16**, 117-122, 1954/55.

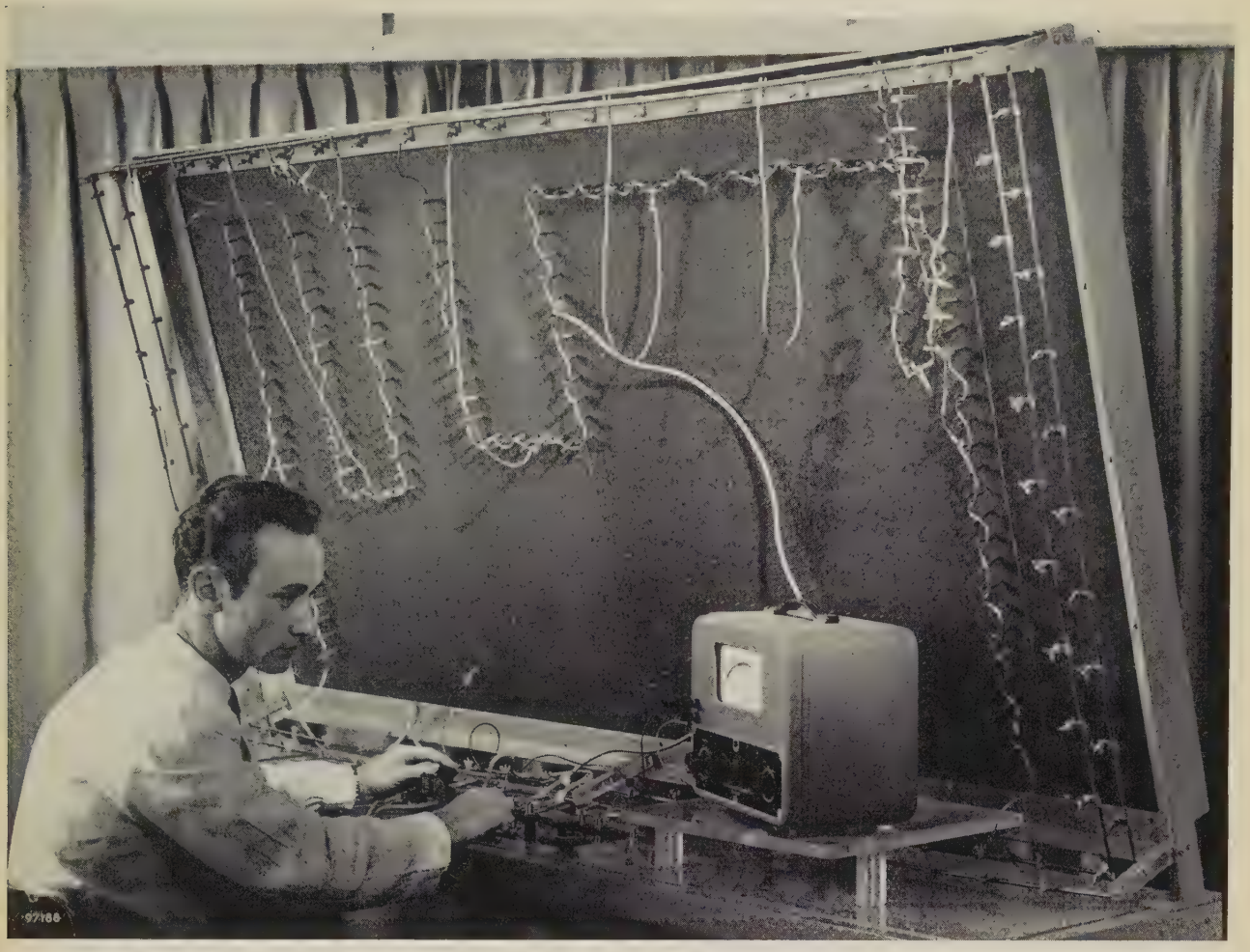

Fig. 9. The resistance network is mounted on the back of a large board of insulating material. The silver-plated contacts that are visible on the front of the panel are the junctions of the network. The electrode configuration seen on the board corresponds to a problem dealt with in this article by way of example. Lengths of 2 mm copper wire, representing electrode outlines, are attached to the appropriate contacts with metal clips. Electrical potentials are applied to these electrode models via heavy copper strips lying along the edges of the network. In order to prevent differences of potential arising along the electrode outlines, each is linked to its copper strip by more than one wire. In the photograph the user has his right hand on one of the knobs of the decade potentiometer; with his left hand he is pressing a key that enables him to check that the needle of the instrument he is watching is giving a null reading.

great sensitivity (readings down to 2 μV can be obtained) with a high internal resistance (0.6 MΩ). The "null current" is therefore less than about 3×10^{-12} A, which is so small that it makes no perceptible difference to the potential distribution. If it was other than very small it could give rise to appreciable errors, particularly in measurements on the axis of symmetry, where the highest-valued resistors lie.

The potentiometer must be very accurate, as its errors show up unchanged in the results. The potentiometer employed had an average accuracy of 1 in 10^5.

A photograph of the resistance network appears in *fig. 9*.

Fields of infinite extent

The region throughout which the required function is present is by no means always enclosed by a boundary such as s_3 in fig. 2. Often it extends to infinity, φ approaching a constant value φ_∞. One can proceed as follows in such cases. First of all, the electrodes are plotted on the network on a scale so small that the junctions around the edge correspond to grid points where φ is already fairly close to φ_∞. All the junctions around the edge are joined up and given a potential corresponding to φ_∞. The simulated electrodes are given potentials in proportion to those of the actual system and an equipotential curve, just enclosing the area within which φ has to be found, is then determined by measurement. Subsequently the scale is increased in such a way that it is still just possible to accommodate the equipotential curve thus found — whose potential is now known — on the resistance network; from then on this curve is treated as an electrode. A similar method can

be employed when it is desired to investigate only part of the region where φ is present, and to plot it on a very large scale, so that one or more electrodes or parts thereof fall outside the resistance network.

The same measurement procedure can be followed as before, one of the electrodes being given a potential differing from that common to other electrodes, and the nett potential distribution being found by linear combination of the results of successive measurements under these conditions.

It is often possible in practice to employ less laborious methods for circumventing the limitations of the resistance network due to its finite dimensions. We shall return to this point when discussing one of its applications.

Example of an application: the determination of the cut-off voltage and maximum cathode loading of electron guns

Often potential distributions are determined to serve as basis for the calculation of electron paths. Here we shall deal with a different example, namely the measurement of potential distributions within tetrode electron guns for cathode-ray tubes as a step towards determining the cut-off voltage and the maximum cathode loading. These two quantities are of importance in the design of electron guns.

For our present purposes an electron gun can be stylized as a set of parallel flat electrodes of infinite extent. The simplest form of gun (the triode gun in *fig. 10*) comprises three electrodes, the cathode K, the grid G and the anode A. Grid and anode have a circular aperture. The centres of the apertures lie on an axis perpendicular to the cathode, and consequently the potential field exhibits rotational symmetry about this axis. The anode has a positive voltage V_A, of 15 kV, say, with respect to the

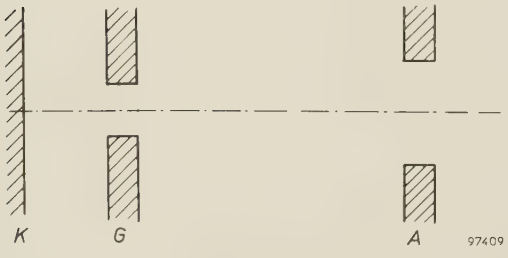

Fig. 10. Diagram to show the arrangement of electrodes in a triode gun. K cathode. G grid. A anode.

cathode. The grid voltage V_G (which is also measured with respect to the cathode) serves to modulate the beam current I issuing from the gun. For a given anode voltage V_A, V_G can be adjusted to a value such that the beam current is reduced to zero. This V_G value is always negative, of course; it is termed the cut-off voltage V_c. It is an important quantity, determining the maximum signal voltage that may be applied to the grid without its becoming positive (see *fig. 11*). Moreover, there is a simple relationship between V_c and the maximum current I_{max} that the gun can deliver under these conditions, viz. [14]):

$$I_{max} \approx 3 \times 10^{-6} \; V_c^{\frac{3}{2}} \text{ ampere} \quad . \; . \; . \quad (21)$$

(V_c in volts). It is therefore desirable that some method should be available for determining V_c from

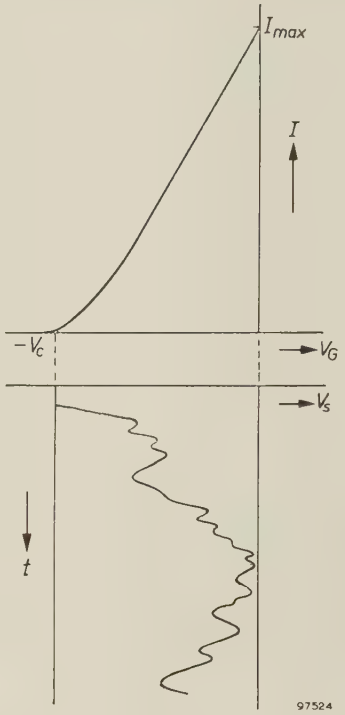

Fig. 11. The above curve showing the beam current I of a triode gun as a function of the grid voltage V_G, the anode voltage being constant, is a normal I_A-V_G characteristic for a triode. If excessive spot "blooming" is to be avoided, the signal voltage must not be allowed to push V_G above zero (otherwise grid current would start to flow). The "blacks" in the signal current correspond to $-V_c$, the cut-off voltage. Hence V_c also represents the maximum signal voltage.

the dimensions of the gun and from the voltage applied to the anode.

For this purpose we employ a graphical method, the graphs being derived from measurements performed with the resistance network. Use can be made of these graphs in the design of tetrode guns. A tetrode gun has a fourth electrode which is mounted close to the grid in the space between grid and anode (*fig. 12*). The fourth electrode is given a positive potential of about 300 V and is known as the "first anode", the original anode being called "final anode" in order to distinguish between the two. In practical cases the voltage on the final anode has but little influence on the cut-off voltage and the beam current, and consequently we only

[14]) See for example M. Ploke, Elementare Theorie der Elektronenstrahlerzeugung mit Triodensystemen, Z. angew. Phys. **3**, 441-449, 1951 and **4**, 1-12, 1952.

need consider the triode portion K-G-A_1. Even so, the system possesses properties different to those of a normal triode gun. In the latter, grid and anode are comparatively far apart. Consequently the field between these electrodes is more or less uniform and

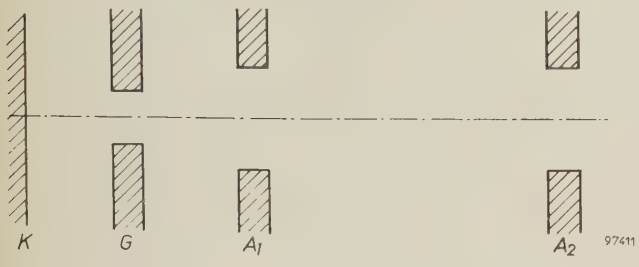

Fig. 12. In a tetrode gun the first anode A_1, which is given a potential of about 300 V, is placed close to the grid G. The final anode A_2 carries a high tension of about 16 kV.

its strength is given by the potential difference between grid and anode divided by the distance separating those electrodes. Hence this ratio determines the cut-off voltage, the diameter of the anode aperture playing no part at all. In a tetrode gun, on the other hand, the clearance between grid and first anode is small and the field between them is anything but uniform. Consequently the potential difference and distance between these electrodes each exercise a separate effect, and the size of the aperture in the first anode also has an influence on the cut-off voltage.

Let us take the following for the potential distribution along the axis (assuming $\varphi(0) = 0$):

$$\varphi(z) = V_{A1} f(z) + V_G h(z) . \quad . \quad . \quad . \quad (22)$$

$f(z)$ represents the variations in potential along the axis when $V_{A1} = 1$ and $V_G = 0$, and $h(z)$ represents the corresponding distribution when $V_G = 1$ and $V_{A1} = 0$ (*fig. 13*). The beam current will be cut off when the current density in the centre of the cathode (where current density, as a function of position on the cathode, always exhibits a maximum) has become zero. Let us assume that the electrons have no initial velocity on quitting the cathode; if that is so, the beam current will be cut off the moment that the potential gradient at the centre of the cathode becomes zero, for the field strength $E(0)$ will then be zero at that point. Since E along the axis is $-\partial\varphi/\partial z$, we can find the field strength at the cathode centre by differentiating (22) with respect to z and putting $z = 0$:

$$E(0) = -\{V_{A1} f'(0) + V_G h'(0)\} . \quad . \quad (23)$$

$E(0)$ becomes zero when $V_G = -\{f'(0)/h'(0)\} V_{A1}$; hence the cut-off voltage is

$$V_c = \frac{f'(0)}{h'(0)} V_{A1} = D V_{A1} . \quad . \quad . \quad . \quad (24)$$

The quantity $D = f'(0)/h'(0)$ is known as the "penetration coefficient" or "Durchgriff".

With the aid of the resistance network, curves $f(z)$ and $h(z)$ were determined for many different combinations of electrode dimensions and separations, D being derived from the slopes of these curves at the cathode. It was found that their slopes at this point hardly alter in consequence of a change in the axial thickness of the first anode; hence D is virtually independent of that dimension. The discovery was welcome, because it meant one parameter less to be considered. Our investigations were limited to the case where the openings in grid and first anode have the same diameter. Since it is only the ratios between electrode dimensions that matter, the parameters are finally reduced to three. The overall results of the measurements are displayed in the set of graphs appearing in *fig. 14*. From these graphs one can determine the penetration coefficient of a gun whose dimensions are known; V_c, the cut-off voltage, can then be calculated with the aid of (24).

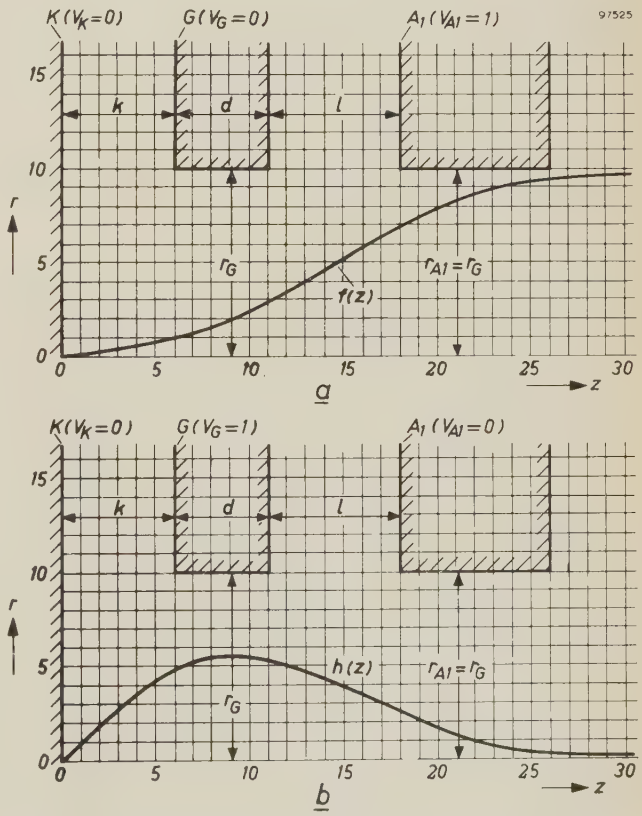

Fig. 13. *a*) Potential distribution $f(z)$ along the central axis in the triode portion of a tetrode gun when $V_G = 0$ and $V_{A1} = 1$. *b*) Potential distribution $h(z)$ along the same axis when $V_G = 1$ and $V_{A1} = 0$.

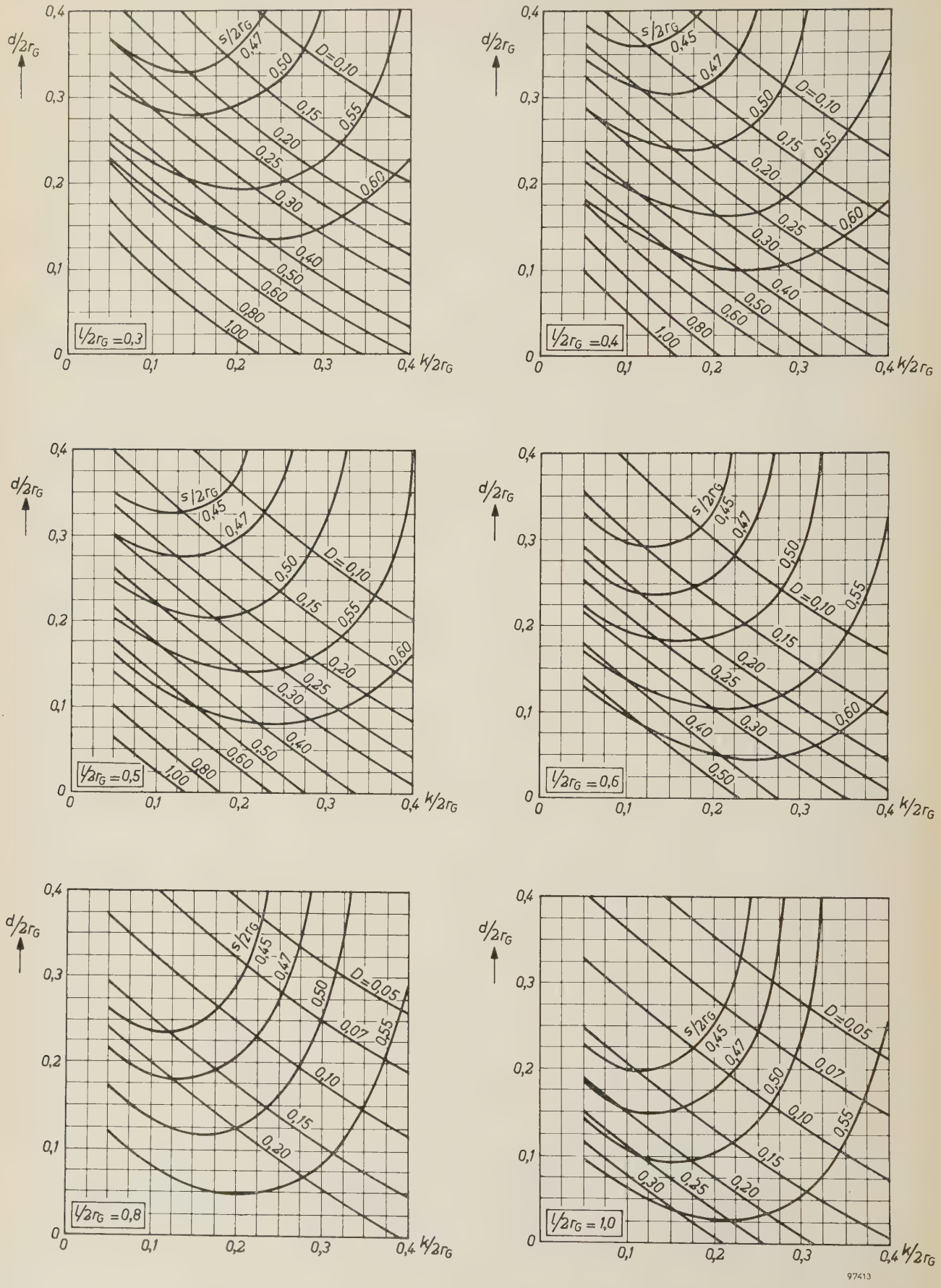

Fig. 14. Graphs allowing D, the "penetration coefficient", and s, the "equivalent anode distance", to be determined for an electron gun of given dimensions. For the meaning of the letters see fig. 13.

A second important quantity provided by the same measurements is the current density in the centre of the cathode (the maximum cathode loading). It is impermissible for the current density to exceed a certain value at this point, and this naturally constitutes a limit in design. Using a simplified theory, Ploke [14]) has derived the following for the current density at the cathode centre:

$$j(0) \approx 4.8\times10^{-3}\,(I\,V_c)^{\frac{3}{5}} \times s^{-2}\ \mathrm{A/mm^2}, \quad . \quad (25)$$

in which I is measured in amperes and V_c in volts, and where

$$s = \frac{1}{h'(0)}\ \mathrm{mm}.$$

The parameter s is sometimes called the "equivalent anode distance". The reason for the name is that if a potential difference of $V_c + V_G$ exists between cathode and anode in a plane parallel diode ($V_G < 0$), the field strength in the intervening space becomes equal to $E(0)$ when the anode-to-cathode distance is s. This can be deduced from (23) and (24).

In order to calculate D we had to determine the slope $h'(0)$ at the cathode; we can now use it again to calculate s. Curves from which s can be read off for a gun of known dimensions also appear in fig. 14. Knowing s, we can work out from (25) the maximum cathode loading for any value of beam current.

Numerical example

Suppose that we want to determine the cut-off voltage and the maximum cathode loading for a tetrode gun with the dimensions $k = 0.15$ mm, $d = 0.15$ mm, $2r_G = 2r_{A1} = 0.75$ mm and $l = 0.35$ mm (see fig. 13), and with an accelerator anode potential of $V_{A1} = 300$ V.

By calculation, $k/2r_G = 0.20$, $d/2r_G = 0.20$ and $l/2r_G = 0.466$. The values of D and $s/2r_G$ appropriate to these values of $k/2r_G$ and $d/2r_G$ are now determined from the two graphs in fig. 14 for $l/2r_G = 0.4$ and 0.5. We then find by linear interpolation that, for $l/2r_G = 0.466$, D is 0.23 and $s/2r_G$ is 0.51, from which it follows that s is 0.39 mm. Formula (24) gives $V_c = 0.23\times300 = 69$ V for the cut-off voltage and formula (25) gives $j(0) = 0.40\ I^{3/5}$ for the maximum cathode loading. If for example the gun provides a beam current of 100 μA, so that $I = 10^{-4}$ A, the maximum cathode loading will be $j(0) = 1.6\times10^{-3}$ A/mm^2.

The limited dimensions of the resistance network

Figs. 8 and 9 are related to the example just worked out; they represent, however, the more general case in which the grid and first anode apertures are unequal. We may now make some observations concerning the measures taken to allow for the fact that the resistance network is not infinitely large in relation to the electrode models plotted upon it. It will be seen from these two figures that the outline of the first anode has been extended along two edges of the network, the junctions on CD and DE having been wired together. As already stated, the results of the measurements are much the same whether the final anode is present or not, and we can accordingly leave it off the network. In these circumstances any point beyond the first anode and at some distance from its aperture will have a potential equal to that of the first anode itself. This will certainly be more or less true of points in space corresponding to the junctions along CD and DE. There is therefore no objection to giving these junctions the said potential. If they were not joined up, one would be completely in the dark about possible errors arising because the portion of the network to the right of the first anode is, as it were, left floating. In the event, the junctions along CD and DE have been short-circuited; and while it is true that the outline thus traced no longer conforms to that of the first anode under investigation, one does at least know that the discrepancy will not give rise to any serious error.

Our second observation concerns the interelectrode spaces between K and G and between G and A_1. The network only extends over a comparatively short distance in the radial direction; what sort of error does this give rise to? The results of measurements of potential in the inter-electrode spaces along the edge of the network (i.e. for maximum r) are reassuring, for the variation in the z-direction proves to be linear within the required limits of accuracy. This means that the height of the network (its extent in the r-direction) is adequate.

Implications of the finite mesh width

Obviously, the mesh with a of the theoretical grid cannot be reduced indefinitely, as this would lead to ever larger models on the resistance network. Hence the network will only provide approximate solutions to the problems worked out on it. In general, it is impossible on the basis of purely theoretical reasoning to estimate this fundamental error with any degree of accuracy. To get some idea of this accuracy, the network can be used for working out a problem whose exact solution is known, the potential distribution found with the network being compared with the known distribution. Alternatively, measurements can be performed for ever smaller mesh widths, a better approximation to the correct solution then being found by extrapolation [15]) [16]).

Cylindrical capacitor

Here we shall give some results of investigations relating to a cylindrical capacitor [17]). For such a capacitor the potential distribution can be worked out exactly. Further, it is possible by calculation to find the solution that would be obtained with an

---

[15]) L. F. Richardson, How to solve differential equations approximately by arithmetic, Math. Gazette **12**, 415-421, 1924/25.

[16]) R. Culver, The use of extrapolation techniques with electrical network analogue solutions, Brit. J. appl. Phys. **3**, 376-378, 1952.

[17]) J. C. Francken, Electron optics of the image iconoscope, thesis Delft, 1953, p. 36 et seq.

"ideal" resistance network. The error due to the finite mesh width can then be determined by comparing the latter solution with the exact one. Other errors, like those due to inaccuracies in resistor values or in the adjustment of the bridge, are thus excluded in this comparison.

If the ratio of the radii of the inner and outer electrodes is 1 : 10 and if the mesh width is made equal to the inner radius, the error is found to be, at worst, —0.7% of the voltage across the electrodes (the worst error arises at the grid points closest to the inner electrode). Near the outer electrode the error is only about —0.07%. If the mesh width is halved, the errors become about —0.2% and about —0.02% respectively. By correction of results by extrapolation the errors can be brought down to about —0.03% and about —0.001% respectively.

The problem of the cylindrical capacitor was also worked out on the actual resistance network, with the two mesh widths mentioned above. After correction by extrapolation, the results for junctions near the inner and outer electrodes differed from the calculated true values by —0.035% and —0.008% respectively. Differences between the experimental values and those calculated from the "ideal" network are due to the other errors referred to above, and have nothing to do with finite mesh width.

An electrostatic lens

Extensive investigations were also made into the part played by the finite mesh width when the problem is to determine the potential distribution along the axis of an electrostatic lens as in *fig. 15a*.

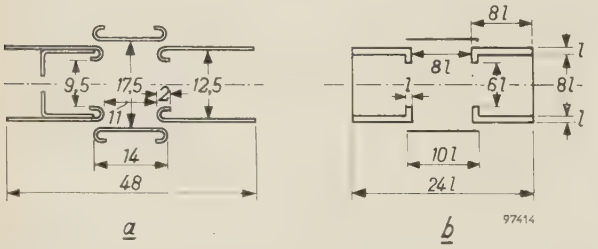

Fig. 15. *a*) Lens of a type used in electrostatically focussed picture-tubes. The electrodes to right and left have the highest potential in the tube; the middle one is at cathode potential. *b*) Shape of the same lens when stylized for the purpose of investigating the effect of the finite mesh width on resistance-network measurements of the potential distribution along the lens axis. The electrode dimension l has been selected as the characteristic length to fix the mesh number, i.e. the scale on which the lens is to be modelled on the network (mesh number $n = l/a$, a being the mesh width of the grid; see fig. 2).

This type of lens is used in television picture-tubes. The two narrower electrodes have the highest potential present in the tube; the middle electrode is at cathode potential. For the purpose of the investigation the lens was stylized, being given the symmetrical shape indicated in fig. 15*b*. In the stylized lens the ends of the outside electrodes are closed by conducting plates.

The electrodes are "capped" in this way for the same reason that led us to introduce further connecting wires into the model of the first anode dealt with above. Here as before, we have to consider the inter-electrode gaps. It is possible, amongst other things, to short-circuit the entire upper edge of the network and to give it zero or unit potential. It proves that this has no appreciable effects on the results. It may be concluded that the limited size of the network in relation to the spaces between the electrodes, does not prejudice the reliability of the measurements.

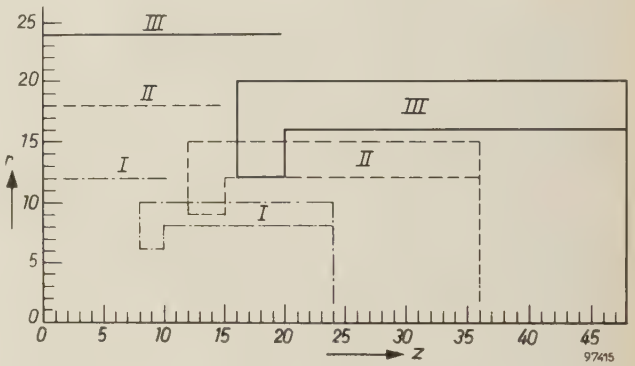

Fig. 16. The lens of fig. 15*b* plotted on the resistance network. Symmetry makes it unnecessary to model more than a quarter of the lens assembly. Measurements were carried out on three electrode models (one at a time, of course) plotted with mesh numbers of 2, 3 and 4, and marked *I*, *II* and *III* respectively in the diagram.

The left-hand edge of the resistance network is made a mirror plane of symmetry by doubling the values of the resistors forming this edge (cf. the

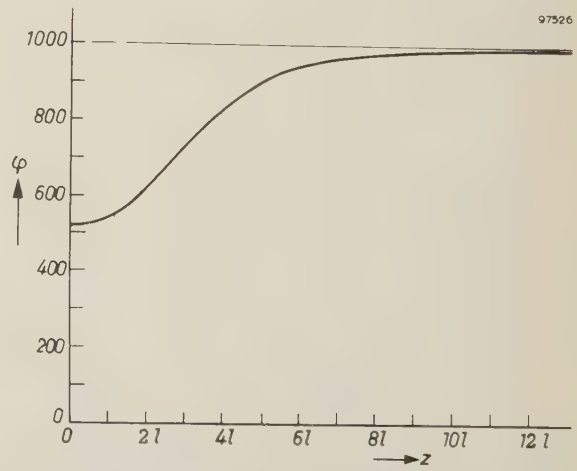

Fig. 17. Variation in potential along the axis of the lens in fig. 15*b*, as determined by means of a resistance network. The scale of this graph is too small to allow any distinction to be made between the slightly different results obtained from measurements on the three different models.

mirror plane along the z-axis in fig. 6*b*). In consequence, only a quarter of the lens had to be simulated on the network. The proportions of the stylized electrodes were so chosen that the lens could be plotted with "mesh numbers" that were in the proportions of 2 : 3 : 4. The "mesh number" is the ratio n between l, one of the dimensions of the lens, and a, the mesh width of the grid. Any dimension of the lens can be chosen for this purpose provided that it is consistently adhered to. Our choice is indicated in fig. 15*b*. The greater the mesh number, the finer is the grid and the bigger is the electrode model on the network (*fig. 16*). The potential values measured along the lens axis are plotted in *fig. 17*. The curve as drawn here is not thin enough to reveal divergencies arising from the use of the three mesh numbers.

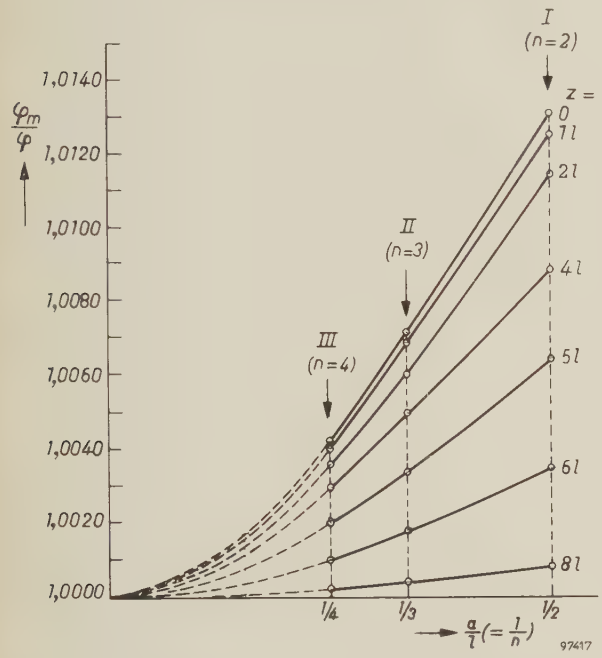

Fig. 18. The relative error (the measured value φ_m divided by the "correct" value φ) in the potential distribution curve of fig. 17, plotted as a function of the mesh width a. The quantity a/l along the abscissa is the reciprocal $(1/n)$ of the mesh number. The seven curves are appropriate to seven points along the z-axis. Each has been drawn through three points determined by resistance-network measurements on three models (*I*, *II* and *III* in fig. 16). Even when the coarsest grid is used the errors remain small.

The three values found for each point along the axis were used to work out, by Culver's method of extrapolation [16]), a value regarded as correct. The three measured values of each set were divided by the "correct" value and the results plotted in *fig. 18*; the three points of each set are joined by a smooth curve. Sets of values appropriate to several points on the z-axis are given. The figure clearly reveals how slight an effect is exercised by the finite mesh width on the results of measurements with the resistance network.

Summary. The resistance network has won a place beside the electrolytic tank as an aid to the solution of Laplace's equation for given boundary conditions. Two kinds of network have practical importance. The first is useful for solving two-dimensional problems, the second for solving three-dimensional problems where rotational symmetry exists. In either case Laplace's equation reduces to a differential equation involving two independent variables only. The network is built up of resistors, four of which meet at each junction. The junctions correspond to the grid points of a hypothetical square grid which is imagined to have been set up in the field space. Junctions corresponding to boundaries are given potentials proportional to those values which the boundaries are known to have. Provided the resistors composing the network have the right values, the remaining junctions will then acquire potentials that are approximately proportional to the required potential function. Discrepancies from the actual values decrease as the mesh width of the grid is reduced to zero. Conditions which must be satisfied by the resistances composing the network, in both the two-dimensional and in the rotationally-symmetric three-dimensional case, are worked out in the course of the article. An example of the employment of a network for rotationally-symmetric three-dimensional problems is given in which curves are derived which allow the cut-off voltage and maximum cathode loading of tetrode electron guns to be determined. Finally, examples are given to show that the errors due to the finite mesh width are very small.

VECTOR-ELECTROCARDIOGRAPHY

by G. C. E. BURGER *) and G. KLEIN.

621.3.012.1:612.17:612.172.4

Developments in electronic engineering enable the physician to apply increasingly refined physical methods to problems of diagnosis. One of these methods, which has made great strides in the last 20 years, is the investigation by means of the vector-electrocardiograph of the electrical phenomena accompanying the contraction of the heart. The article below describes one of the vector-electrocardiographs built in the Philips Research Laboratory at Eindhoven and in use at the Philips Health Centre. In the introduction the physical principles of vector-electrocardiography are touched on and a brief discussion is devoted to the nature of the electrical phenomena concerned and the relation between vector-electrocardiography and conventional electrocardiography from which it evolved.

Introduction

A valuable aid in cardiology is the study of the electrical phenomena that occur during the contraction and subsequent relaxation of the heart muscle. These electrical phenomena are related to the manner in which the stimulus giving rise to the contraction is propagated over the heart muscle. Changes in these electrical phenomena enable the cardiologist to learn something about the cardiac disorders responsible for the changes, such as the presence of an inactive part (infarction) or an enlargement (cardiac hypertrophy) of the heart muscle. Purely mechanical disorders (openings in the septum, valvular deficiencies) are not primarily included in this category, although they are not infrequently the cause of other disorders which in turn do manifest themselves by an electrical phenomenon.

Electrical phenomena accompanying muscular contraction

The electrical phenomena referred to are brought about roughly as follows.

In the resting state the wall of every muscle fibre (a membrane) constitutes an electric double layer; the potential of the interior of the fibre is about 60 mV lower than that of the environment (the "medium"). This phenomenon is termed *polarization*. At the position where a stimulus is applied to the fibre, this potential difference — known as the *membrane potential* or *resting potential* — decays very rapidly (in approximately 1 millisecond) and even reverses its polarity to the peak value of about 35 mV; this is known as *depolarization*. As a result of this effect an electric current, which varies from place to place throughout the whole volume of the medium, flows from the intact fibre wall to the stimulated part. This current becomes manifest at the boundary of the medium, in this case the surface of the body, in potential differences between the various points of the surface (*fig. 1*).

The current in the medium can be formally represented as being generated by a galvanic cell whose terminals are at a small distance apart on the centre-line of the fibre (dipole). The positive pole

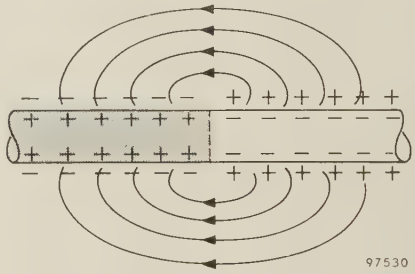

Fig. 1. Schematic representation of a partially stimulated muscle fibre. The non-stimulated part has a potential lower than that of the medium; in the stimulated part (shaded) the potential difference has changed its polarity. This causes a current to flow in the medium.

represents the intact part, the negative the stimulated part. The electric field is now determined by a quantity depending both on the potential difference between the terminals (the electromotive force) and their distance apart, and on the direction of the centre-line referred to; in other words, it is determined by a *vector quantity*.

The current flow implies that the medium surrounding the intact wall, particularly near the edge of the stimulated zone, loses charge, resulting in a drop in the potential difference between the two sides of the wall. This in turn acts as a stimulus, causing the membrane potential here also to change as described above; in other words, the boundary between stimulated and non-stimulated zones propagates itself along the length of the fibre. In regard to the fibres of the heart muscle the velocity of propagation is of the order of magnitude of half a metre per

*) Professor of Public and Industrial Hygiene, University of Amsterdam. Until his recent retirement Prof. Burger was the Director of Medical Services of N.V. Philips.

second. It should be noted that the transition region between the stimulated and non-stimulated part of these fibres is extremely short, and is in any case very small compared with the dimensions of the heart.

Immediately after a certain part of a fibre has entered into the stimulated state, the membrane potential begins to return to the resting value — the repolarization process — which it reaches in about 0.2 second. This relatively slow recovery means that the stimulated part of a fibre could have a length of about ten centimetres if the fibre were only long enough. In reality the length of the fibres is much less. This is one reason why the human heart can be in a completely depolarized state for a short time.

The electrical action of the boundary between a stimulated and a recovered region is analogous to that of the front edge of the stimulated region. The vector quantity associated with the repolarization, however, assumes an appreciable value only after some tenths of a second from the beginning of the stimulus.

An electric double layer with properties corresponding to those of muscle fibres is found, during life at least, in the walls of all biological structures that react to stimuli (nerves, muscles, glands, sensory receptors, etc.). The potential difference is a consequence of the permeability of the membrane, which differs widely for different kinds of ions. The membrane is completely impermeable to SO_4^{2-} ions and to the large organic ions contained in the fibre; to Na^+ it is only slightly permeable, whereas it is relatively highly permeable to K^+ and Cl^-. As a result the various kinds of ion inside and outside the fibre differ considerably in concentration. The membrane potential is virtually equal to the diffusion potential of the K^+ ions. The action of a stimulus causes the permeability to Na^+ ions to become suddenly about 500 times greater, which then far exceeds for a short time the permeability to K^+ ions. Consequently the membrane potential changes sign and becomes virtually equal in magnitude to the Na^+ diffusion potential. Na^+ ions then flow in and K^+ ions flow out.

When the stimulus ceases, the permeability returns to its original value. The K^+ ions diffuse back again through the wall, but the Na^+ ions are now "trapped" inside and are "pumped" out by a metabolic process known as the sodium pump mechanism.

Although the electrophysiological study of the nervous system has made great advances, particularly in the last ten years, it is still not yet known exactly how the Na^+ pump works, nor how it comes about that the application of a stimulus suddenly changes the permeability of the wall to Na^+ ions. The restoration to the resting state also awaits clarification [1]).

The heart vector

The electric field which the heart muscle as a whole gives rise to in the body is the sum of the contributions of each separate fibre. At a large distance from the source this electric field cannot be distinguished from that of a single fibre (dipole) the electromotive action of which is characterized by a vector equal to the sum of the vectors which define the action of each of the fibres belonging to the muscle. In close proximity to the heart this is no longer applicable; here the closest parts of the muscle make a greater contribution to the field at a certain point than the parts farther removed.

This vector sum, which thus defines the electromotive action of the whole heart muscle as manifested at a relatively large distance in the medium, is termed the *heart vector* (*fig. 2*). Because of the complicated way in which the heart muscle is depolarized and repolarized, this vector undergoes marked

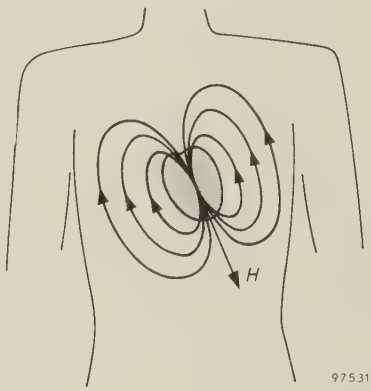

Fig. 2. The electrical action of the heart as manifested at a relatively large distance from the heart in potential differences between the various points of the medium can be described by a vector **H**. During the heart beat this vector varies considerably in magnitude and direction.

changes in magnitude and direction during the heart beat. If we represent the heart vector by an arrow one end of which is at a fixed point, the arrow will thus swing to and fro, while varying in length, around this fixed point during the heart beat. The point of the arrow describes in space an irregular curve, called the *vector-electrocardiogram* (Vcg).

Conventional and vector-electrocardiography

As mentioned, the current flowing through the body gives rise to potential differences between the various points on the surface of the body. These potential differences are of the order of magnitude of 1 mV. With a sensitive and rapidly indicating instrument of high internal resistance, these potential differences can be measured and their variation with time recorded. The result is a conventional electrocardiogram (Ecg). Its appearance varies, of

[1]) A review of the present state of knowledge in this field will be found in A. von Muralt, Neue Ergebnisse der Nervenphysiologie, Springer, Berlin 1958, and in J. C. Eccles, The physiology of nerve cells, Johns Hopkins Press, Baltimore 1957.

course, with the chosen combination of points between which the measurement is made.

Such a combination of two contact points is known as a *lead* or *derivation*. The number of possible leads is obviously unlimited, but for practical reasons the electrodes are applied to a number of standard positions, the oldest of which are the two arms and the left leg. Standard positions have also been selected on the back and chest; sometimes, too, an electrode is let down into the oesophagus. In a complete cardiological examination electrocardiograms are recorded as a rule from a large number of leads.

It should be noted that some leads are not obtained by connecting the instrument directly to two electrodes, but by connecting only one terminal directly to the electrode and the other via resistors of about 5000 Ω to three others placed on the two arms and the left leg. The potential on this terminal is then equal to the average of the potentials on the three electrodes to which it is connected; this does not imply, however, that this average is zero or that it has any other value not varying with time. The leads between electrodes on the arms and the left leg are known as the three *standard leads of Einthoven*. Since the current lines hardly penetrate into the extremities, it is of little consequence where exactly the electrode is placed, which makes it easy to work with these leads.

To obtain good recordings it is of course necessary that the potential differences applied to the instrument should be caused solely by the action of the heart. The patient should therefore be completely relaxed. The potential differences originating from other muscles are often the chief form of interference.

Form of conventional and vector-electrocardiograms in relation to the action of the heart

Before considering the manner in which a vectorcardiogram is recorded, it will be well to take a closer look at the action of the heart muscle and the way in which it manifests itself in electrocardiograms and vectorcardiograms (we shall frequently below use this abbreviated form in place of vector-*electro*cardiogram(graphy)).

As is well known, the heart consists of two parts, the left heart and the right heart, which are separated by a dividing wall or *septum*. Each part has two chambers, i.e. an *auricle* (or *atrium*) where the blood enters, and a *ventricle*, which forces the blood into the relevant arteries. The right heart receives the venous blood depleted in oxygen and pumps it into the lungs, and the left heart receives the oxygenated blood from the lungs and pumps it through the arteries to supply the organs and tissues of the body (*fig. 3a*). Both halves of the heart can in fact be regarded as two separate pumps connected in series (fig. 3*b*). The vascular systems between the two pumps are known respectively as the *lesser* (pulmonary) circulation and the *greater* (systemic) circulation.

The interauricular septum, i.e. the part of the dividing wall between the auricles, is a membrane; the outer wall of the auricles is a fairly thin muscle.

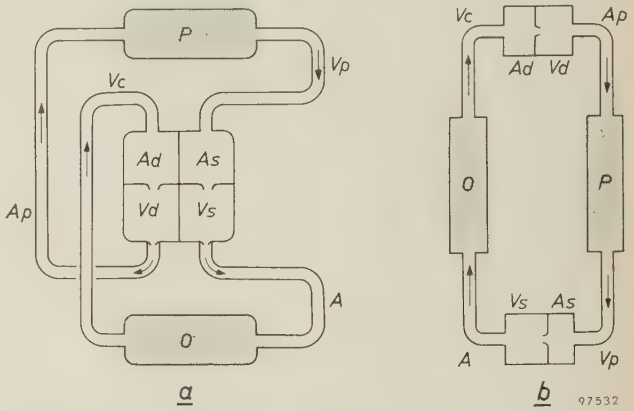

Fig. 3. *a*) Schematic representation of the human circulatory system. *As* left auricle, *Vs* left ventricle, *A* aorta, *O* organs, *Vc* vena cava, *Ad* right auricle, *Vd* right ventricle, *Ap* pulmonary artery, *P* lungs, *Vp* pulmonary vein. *b*) The same with the two halves of the heart drawn separately. These halves constitute simultaneously operating pumps connected in series.

The upper part of the septum between the ventricles is also a membrane, but somewhat lower it goes over into a muscular wall which is integral with the outer wall of the ventricles. This structure is known as the heart muscle or *myocardium*. The upper part is called the *basis*, the bottom part — i.e. the point of the heart — is the *apex* (*fig. 4*).

Depolarization takes place in the following way. The stimulus begins in the *Keith-Flack node* (or

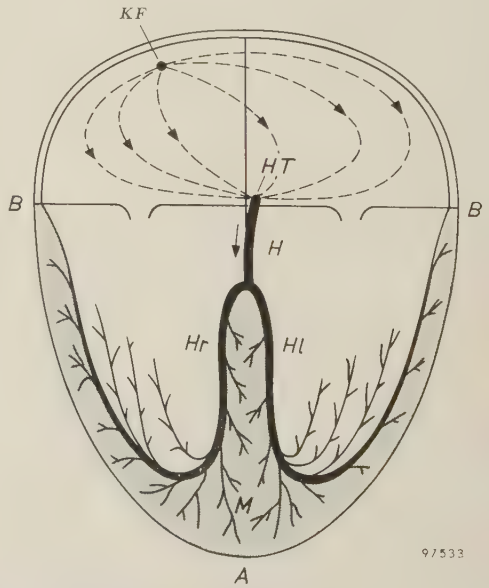

Fig. 4. Representation of stimulus conduction in the heart. *A* apex, *B-B* basis, *M* heart muscle (myocardium), *KF* Keith-Flack node (sino-auricular node), *HT* His-Tawara node (atrio-ventricular node), *H* unramified part of the bundle of His (atrio-ventricular bundle), *Hl* left branch of bundle, *Hr* right branch of bundle.

sino-auricular node) which is located in the wall of the right auricle. From this point the stimulus spreads out over the wall of both auricles. The auricles contract at virtually the same time. At a certain moment the stimulated zone reaches the *His-Tawara node*, which is situated in the septum near the basis of the myocardium (for which reason it is also called the *atrio-ventricular node*). The latter node is the source of a special system of stimulus conduction. This involves a bundle of fibres of non-contractile muscle tissue (known as the *bundle of His* or *atrio-ventricular bundle*) in which stimuli are propagated at about 1 metre per second. The bundle splits into two branches at the point where the septum ceases to be membranous and merges into the myocardium; one branch continues at the left of the septum, the other at the right. These branches in turn split up into large numbers of fibres which extend in the interior of the myocardium over the entire wall of both ventricles, and from which still finer branches extend into the myocardium itself. From these branches of the bundle of His the stimulus propagates itself in the fibres of the ventricular muscle. After some tenths of a second repolarization begins.

The three successive events, depolarization of the auricles, depolarization of the ventricles and repolarization of the ventricles, give rise in the electrocardiogram and the vectorcardiogram to three clearly distinguishable deflections. These are denoted respectively by *P*, *QRS* and *T*. *Fig. 5* shows a normal electrocardiogram obtained by recording the potential difference between the right and left arms. It can be seen that between the three electrical phenomena there are small time intervals during which the potential difference is zero. In the *vectorcardiogram* the three phenomena appear in the form of three loops, the starting and terminal points of which, for a normal heart, lie in the origin. The form of the *QRS* loop, and whether or not this loop returns to the origin before the *T* loop begins, are of great significance to the cardiologist. The form of the *P* loop is, as yet, of no clinical importance.

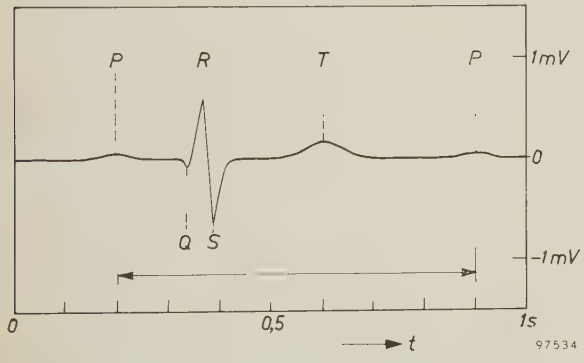

Fig. 5. Electrocardiogram of a normal heart as obtained when the electrodes are applied to the right and left arms. There are three distinct parts which correspond, respectively, to the depolarization of the auricles (*P*-spike), that of the myocardium (*QRS*-complex) and the repolarization of the myocardium (*T*-spike). The length of the arrow corresponds to the time elapsing between two heart beats.

Finally it should again be noted that the heart vector is the sum of a large number of individual vectors differing in direction and magnitude. The vectorcardiogram provides no information on these individual vectors as such. The relation between the direction of the heart vector and the stimulated state of the heart at a given moment should not be over-simplified. The direction of the vector can be simply correlated with the direction in which the change of state is propagated only during the very first beginning of myocardiac depolarization (start of the *QRS* loop) and during the very first beginning of repolarization.

Mathematical principles of vectorcardiography

In vectorcardiography the object is to try and find the form of the heart vector itself — the above-mentioned vectorcardiogram [2]) — rather than to record a number of separate electrocardiograms. Assuming that the electric field appearing at the surface of the body may be regarded as excited by a stationary point-source dipole, only three mutually independent leads are sufficient for this purpose.

Since the dimensions of the heart are not so very small compared with the body, the above assumption only roughly corresponds to reality at places on the surface of the body which are not too near to the heart. Further, just as in ordinary electrocardiography, the electrodes should obviously not be too close together. It is often found convenient to place three of the four electrodes on the extremities and the fourth somewhere on the trunk. We shall return to this subject presently.

The problem of how the magnitude and direction of the heart vector are related to the potential differences between the electrodes — a problem purely of mathematical physics — is solved in the following way [3]). It can be deduced from physical considerations that the relation between the three independent potential differences P_1, P_2 and P_3 and the magnitude of the three mutually perpendicular components X, Y and Z into which the heart vector

[2]) Research in this field was pioneered by H. Mann (Arch. int. Med. **25**, 283, 1920). The first vectorcardiograph was described by H. E. and W. Hollmann, Z. Kreislaufforschung **29**, 465, 1937.

[3]) H. C. Burger and J. B. van Milaan, Brit. Heart J. **8**, 157-160, 1946.

H can be resolved, is linear, and can thus be defined by the formulae:

$$P_1 = a_1X + b_1Y + c_1Z, \quad . \; . \quad (1a)$$

$$P_2 \quad a_2X + b_2Y + c_2Z, \quad . \; . \quad (1b)$$

$$P_3 = a_3X + b_3Y + c_3Z. \quad . \; . \quad (1c)$$

The coefficients a_1 to c_3 are constants which (in addition to being determined by the directions selected for the coordinate axes; see *fig. 6*) are

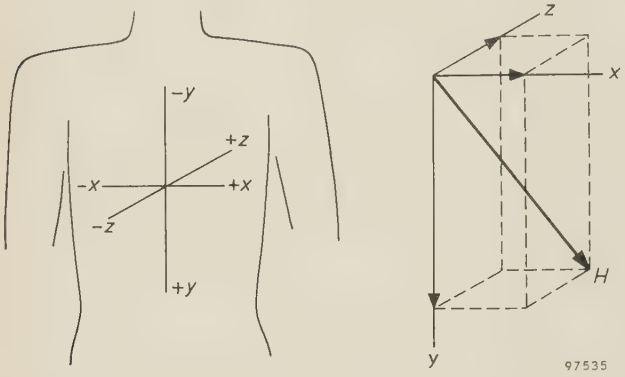

Fig. 6. Coordinate axes selected for vectorcardiography in accordance with the convention adopted by the American Heart Association. XY is the frontal plane, XZ the horizontal plane and YZ the sagittal plane.

determined by the shape of the various parts of the body (muscles, lungs, etc.) and their relative conductivity, by the position where the dipole is imagined to be located in the body, and finally by the position of the electrodes.

The values assumed by the coefficients a_1 to c_3 for various combinations of leads have been determined from measurements on a model of the human body [4]), complete with "lungs" and a "spinal column". The material chosen for the lungs was such that the ratio between their electrical conductivity and that of the rest of the trunk was approximately equal to that believed to exist in the body. The spinal column was made of a very poorly conductive material.

By solving equations (1) we find for the components of the heart vector:

$$X = \alpha_1P_1 + \alpha_2P_2 + \alpha_3P_3, \quad . \; . \quad (2a)$$

$$Y = \beta_1P_1 + \beta_2P_2 + \beta_3P_3, \quad . \; . \quad (2b)$$

$$Z = \gamma_1P_1 + \gamma_2P_2 + \gamma_3P_3. \quad . \; . \quad (2c)$$

Here again, the coefficients α_1 to γ_3 are constants, and can be calculated from a_1 to c_3. Since (2) has general validity, we must always find the same X, Y and Z when comparing measurements made with different leads, provided we use in the calculation those values for α_1 to γ_3 appropriate to the relevant leads. By carrying out comparative measurements of this kind on patients, we thus have a means of verifying the correctness of the values of a_1 to c_3 obtained on the model. In addition we can ascertain in how far the spatial extension of the heart (deviation from an ideal dipole) affects the results.

Recording a vectorcardiogram

In the vectorcardiograph discussed in this article the components of the heart vector are automatically computed from (2). After amplification, the potentials P_1, P_2 and P_3 are fed to a number of potentiometers to obtain the correct fraction of each of the signals. These fractions are then added together. The apparatus does this for each of the equations (2), so that three signals are obtained which are proportional to X, Y and Z.

The form of the earlier-mentioned curve, described in space by the point of the heart-vector arrow, is now found by successively applying combinations of two of the signals to the two pairs of deflection plates of a cathode-ray oscilloscope. If we select, for example, the signals which represent the X and Z components, the screen displays the projection of this curve in the horizontal plane. Analogously, X and Y yield the frontal and Y and Z the sagittal projection. By suppressing the electron beam at regular intervals (e.g. 1/200 sec), time marks are obtained by means of which the points corresponding to each of the various projections can be recognized. By interrupting the recording before the end of the heart beat, or by varying the line thickness between each two time marks, one can determine the direction in which the line is being described.

With some practice it is readily possible to construct from two of the three projections, using the time marks, a wire model corresponding to the three-dimensional curve. The third projection is thus not really necessary, although it is often easier to make the wire model when three projections are available.

Fig. 7 shows various projections and *fig. 8* the wire models derived from them. If the time marks are added to these models, we have an indication of the speed at which the point of the arrow covers the various parts of the loops.

Reverting to the end of the foregoing section, it may be mentioned here that investigations using a number of electrode configurations with known coefficients show that the agreement between the vectorcardiograms obtained with these on any patient is highly satisfactory in a large percentage of cases (70 to 80%) as far as the frontal projection is

[4]) H. C. Burger and J. B. van Milaan, Brit. Heart J. **9**, 154-160, 1947. See also Acta med. Scand. **114**, 584, 1943.

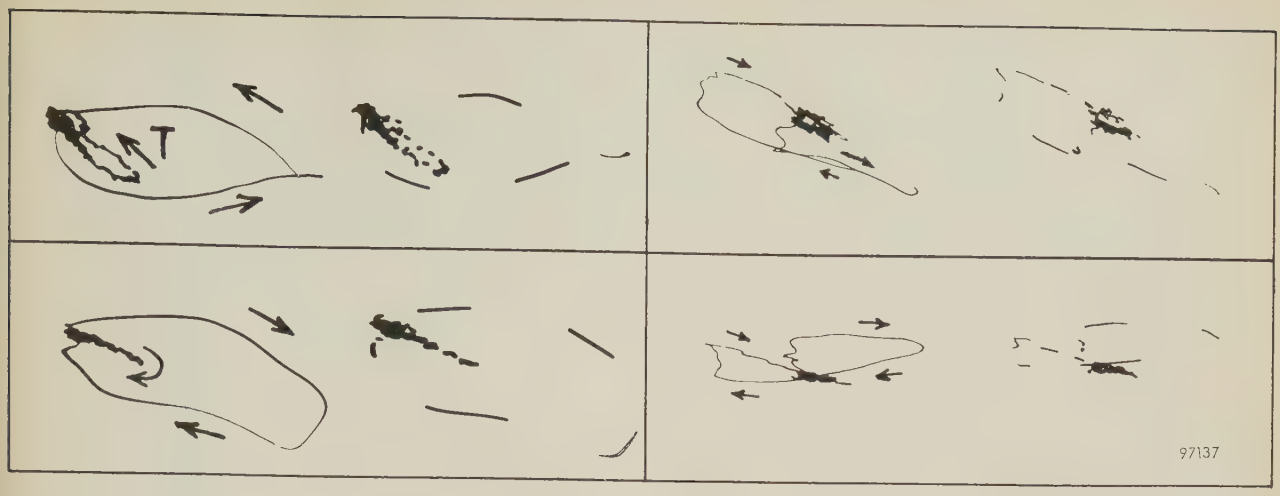

Fig. 7. Horizontal projection (above) and frontal projection (below) of the vector cardiogram of a normal heart (left column) and of a disordered heart (right column). For one of every pair of otherwise identical oscillograms the electron beam is interrupted 200 times per second to obtain time marks.

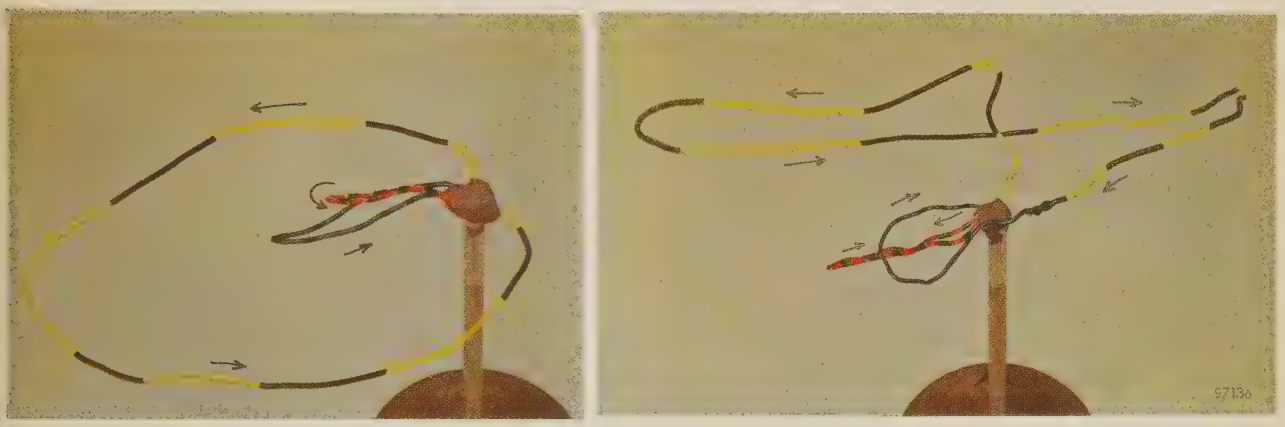

Fig. 8. Vectorcardiogram in the form of a wire model of the normal heart (left) and the disordered heart (right) derived from the two projections shown in fig. 7. The parts (loops) that correspond to the depolarization of the auricles (*P*; red), to the depolarization of the ventricles (*QRS*; yellow) and to the repolarization of the ventricles (*T*; blue) all begin and end at the origin in the case of the normal heart. With the disordered heart, this is not so as far as the *QRS* and *T* loops (yellow and blue) are concerned. The arrows indicate the direction in which the three loops are described. (The patient is viewed obliquely from above with his back to the observer.)

concerned. The agreement is not so good, however, between projections in which the *Z* component (antero-posterior) is involved. Further investigation has shown that the agreement cannot be improved by choosing other coefficients. This suggests that the position of the electrodes does not entirely comply with the physical conditions that must be satisfied if the heart vector (the vector sum of the component vectors) is really to be obtained. Since the electrodes obviously cannot be positioned farther from the heart than the dimensions of the trunk permit, systems employing more than four electrodes are now being studied. The use of more electrodes makes it possible to reduce the influence of the spatial configuration of the heart, i.e. to record the heart vector with less distortion [5]). The instrument about to be discussed was therefore designed for use with both a four-electrode and a five-electrode system. On the

[5]) A system using five electrodes was described by H. C. Burger in Annals New York Acad. Sciences **65**, 1076-1087, 1959, one with six by O. H. Schmidt and E. Simonson in Arch. int. Med. **96**, 574, 1955, and one with seven electrodes by E. Frank in Circulation **13**, 737, 1956.

In a theory put forward by D. Gabor and C. V. Nelson (J. appl. Phys. **25**, 413-416, 1954) it is shown that the fact that the heart is not small with respect to the dimensions of the chest does not in principle prevent the magnitude and direction of the heart vector (and even its position) from being determined with considerable accuracy. For this purpose, however, a very large (theoretically infinite) number of electrodes is needed. With a view to finding a reliable and at the same time practicable method, investigations are proceeding to ascertain how the number of electrodes can be reduced without unduly affecting precision.

other hand it should be noted that where there is poor agreement between the vectorcardiograms obtained with these two lead systems, the deviations are very seldom so serious as to cause significant clinical errors even if the physician were to rely solely on the vectorcardiogram. They do, however, call for some prudence when interpreting a vectorcardiogram.

The geometric relation between vector- and conventional electrocardiograms

The relation between the vectorcardiogram and conventional electrocardiograms obtained with three leads is given analytically by formula (1). If we realize that the potential difference P_1 in formula (1a), for example, is a *scalar* quantity, and that X, Y and Z are *vector* components, we can conclude that a_1, b_1 and c_1 must necessarily also be the components of a vector $\mathbf{p}_1$. P_1 is the *scalar product* of the vectors $\mathbf{p}_1$ and $\mathbf{H}$. Likewise P_2 is equal to the scalar product of $\mathbf{p}_2$ and $\mathbf{H}$, and so on. The vectors $\mathbf{p}_1$ etc. are called *lead vectors*.

On the other hand the magnitude of the scalar product of two vectors can be found by multiplying the magnitude of one of the vectors by the magnitude of the projection on to this vector of the other. Thus:

$$P_1 = p_1 H \cos \varphi, \quad \ldots \ldots \quad (3)$$

where φ is the angle between $\mathbf{p}_1$ and $\mathbf{H}$ and p_1 and H their modulii. If we now construct a tetrahedron the direction and length of three of whose edges correspond to those of the lead vectors $\mathbf{p}_1$, $\mathbf{p}_2$ and $\mathbf{p}_3$, we can deduce from the above that we shall find P_1 by projecting the heart vector $\mathbf{H}$ on the edge $\mathbf{p}_1$ (a_1, b_1, c_1) and by multiplying the length of the projection (which is $H \cos \varphi$) by the length of this edge, and so on.

Of course we can construct such a tetrahedron for any four electrode positions. We select three leads in such a way that they have one electrode in common, and we construct the tetrahedron such that the lead vectors meet in one corner. By keeping one point fixed when changing over from one set of four to another set of four, we obtain a surface formed by the corners of the tetrahedra, each point of that surface corresponding to a point on the surface of the human body. We have then transformed the latter surface (in the empirical space) into a surface in the electrical image space. The line connecting two points on this surface is thus the lead vector for the two corresponding points on the human body. In general this vector evidently has an entirely different direction and magnitude from the line connecting the relevant contact points in the empirical space.

By way of illustration we shall take a simple two-dimensional example (*fig. 9*). It will be obvious that in this example both the imaginary heart vector and the two lead vectors each have only two components; we denote these respectively by X and Y, a_1 and b_1, and a_2 and b_2. The above-mentioned tetrahedron is reduced here to a triangle (whose position in the XY plane, with respect to the origin, is quite arbitrary). The figure shows how the magnitude and direction of the triangle sides can be derived from the values of a_1 to b_2, and also how one can find from the vectorcardiogram the conventional electrocardiograms that would have been obtained from the leads in question. It can be seen that the corresponding spikes in the conventional electrocardiograms do not occur simultaneously. Their sequence is determined from the direction in which the heart vector rotates.

A vectorcardiograph for clinical use

We shall now discuss a vectorcardiograph, built in Eindhoven for use in the Philips Health Centre, which is designed to operate with two lead systems and which can be moved from one place to another as required. The first lead system is one in which electrodes are placed on the left leg, the two arms

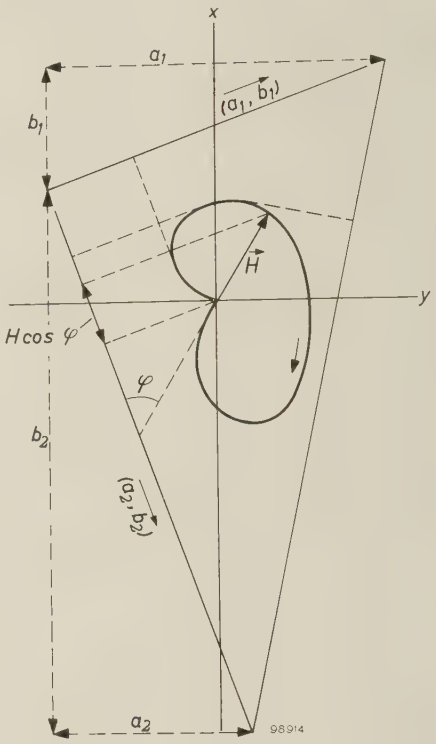

Fig. 9. Two-dimensional illustration of the relation between the heart vector $\mathbf{H}$ and the potential P_i produced between a given pair of electrodes. There are here two independent potentials P_1 and P_2. The appertaining leads (derivations) each give rise to a lead vector having components a_1, b_1 and a_2, b_2, respectively. These form a triangle (capable of parallel movement in the XY plane). The magnitude of P_1, for example, is found geometrically by projecting $\mathbf{H}$ to the relevant lead vector and by multiplying the length of the projection ($H \cos \varphi$) by the magnitude of this vector. It is seen that such a projection and hence P_i will reach its maximum value at different times for all three leads.

and on the middle of the chest in line with the top of the arm pits. The second system uses an additional electrode which is placed on the back at the height of the seventh vertebra, 2 cm left of centre. The apparatus (*fig. 10*) is equipped with a cathode-ray tube (screen diameter 13 cm), on which the spot can describe successively the frontal, the horizontal and the sagittal projection of the vectorcardiogram. A block diagram of the apparatus is shown in *fig. 11*. The potentials L, F, B and W which the left arm, the left leg, the chest and the back, respectively, have in relation to the right arm, are each separately amplified by the four amplifiers A_1 to A_4. The amplified signals are fed to the mixing

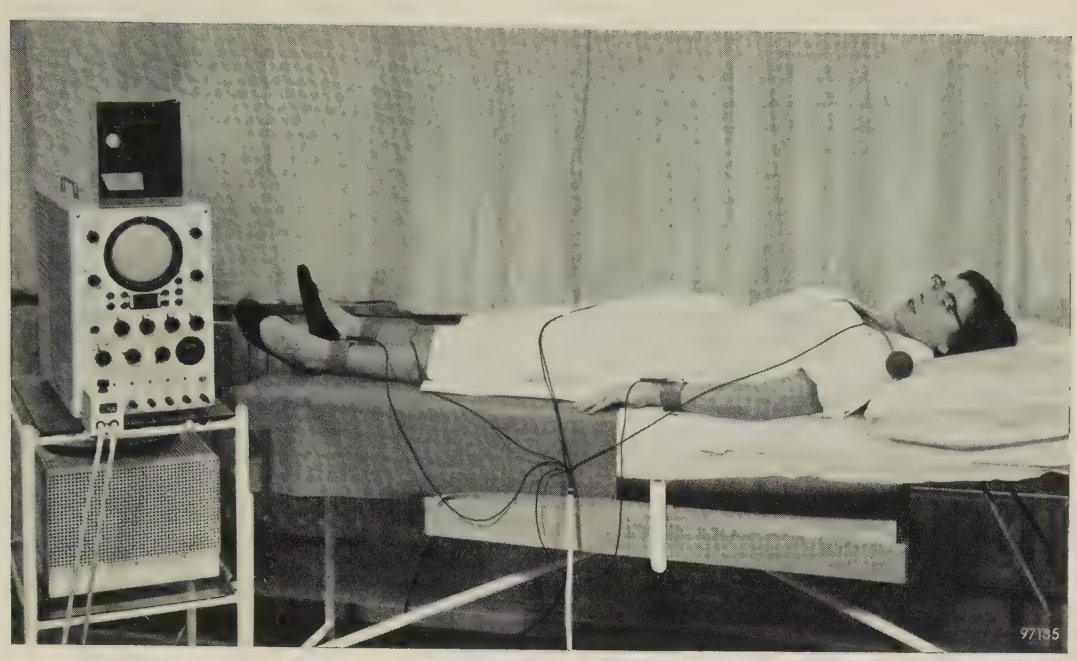

Fig. 10. The vectorcardiograph in use. Two cords can be seen connected to the instrument. One leads to the patient shown in the photograph, the other can be used for connecting a second patient whilst the recordings of the first are made. This makes the apparatus better suited for routine examinations. Each cable contains six conductors, five of which are connected respectively to the right leg (by which the patient is earthed), the right arm (the common point of all leads), the left arm, the left leg and the chest. The sixth can be connected to a dorsal electrode. In the photograph it is not in use (and for this reason is connected to the right arm). The dorsal and chest electrodes are applied by means of a sucker. The power-supply circuits are contained in a separate housing, shown below the oscilloscope in the photograph. The oscilloscope also houses the vectorcardiograph circuits proper. The bracket on which the camera can be mounted is folded back.

circuit M, which "computes" and adds the terms of the equations (2). Of the three signals produced by this circuit, which are proportional to the X, Y and Z components of the heart vector, two are applied, after further amplification by B_1 and B_2, to the horizontal and vertical deflection plates, respectively, of the oscilloscope, which thus always displays a projection of the vectorcardiogram. The beam modulator C contains three circuits. The first periodically suppresses the oscilloscope beam to produce time marks on the screen. The second varies the intensity of the beam with the writing speed; in the first place this prevents the beginning of the trace — where the spot remains for a relatively long period — from causing a large black mark on the film at that position, which would make it impossible to determine the origine of the vectorcardiogram; in the second place it prevents the slow parts of the trace from appearing exceptionally thick. The third circuit makes it possible to display only part of the projection while suppressing the remainder; this also enables the observer to determine the direction in which the vectorcardiogram is described.

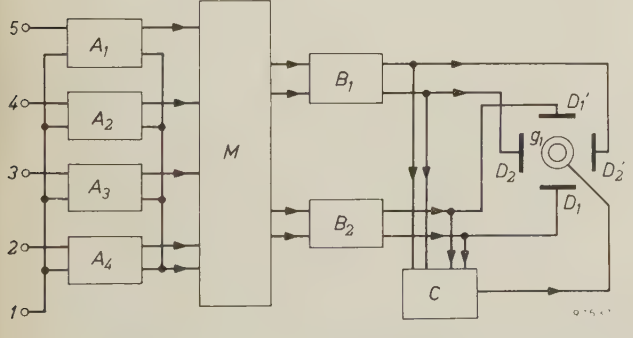

Fig. 11. Block diagram of vectorcardiograph. All potentials are measured with respect to the right arm (terminal *1*), namely those of the left arm, the left leg, the chest and possibly the back. A_1 to A_4 pre-amplifiers, M mixing circuit, B_1 and B_2 output amplifiers, D_1-D_1' and D_2-D_2' deflection plates of oscilloscope, g_1 CRT control grid, C beam modulator.

We shall now discuss each of these components in turn, after which we shall touch on ways and means of suppressing external interference.

Pre-amplifiers

The pre-amplifiers in a vectorcardiograph are required to amplify the potential difference of two points, neither of which are at earth potential, in such a way that the average of the potential on these points in no way affects the output signal. This requirement, which applies equally to a conventional electrocardiograph, is necessary not only because the action of the heart causes the potential of the

contact points to deviate from earth potential, but also because of the occurrence of interfering signals (hum) which cause the potential of the whole body to differ from zero. Further, a high input impedance is required because 1) the interior of the body cannot be regarded as a voltage source of low internal resistance, and 2) a current flowing from the body to an electrode plate encounters a resistance of several kΩ in passing the skin, even when the skin is treated with an electrode paste [6]). Finally, the amplifier must not amplify constant voltages, arising among other things from the use of electrode paste, although the lower limit of the frequency characteristic should not be higher than approximately 0.1 c/s.

The circuit designed for the amplifiers A_1 to A_4 (fig. 11) and which meets the requirements mentioned to a high degree, is shown in *fig. 12b*. The first stage (under the dashed line) can be regarded as derived from a simple pentode difference-amplifier (fig. 12*a*) in the following way: 1) the pentodes are each replaced by a series (cascode) arrangement of two triodes; 2) the common cathode resistor is replaced by a triode *III*; 3) the circuit supplying the grid bias for the triodes *Ib* and *IIb* (and which is comparable with the battery supplying the screen-grid voltage in the pentode amplifier) consists of a triode *IV* connected as a cathode follower. This stage has a rejection factor of more than 10^4, that is to say, the change in the *average* potential of g_1 and g_1' must be at least 10^4 times larger than the potential *difference* of g_1 and g_1' in order to make the same contribution to the output signal. The average potential of $\frac{1}{2}(V_{g1} + V_{g1}')$ can thus vary within a wide range compared with that in which $V_{g1} - V_{g1}'$ varies, without this being noticeable in the output signal [7]).

The second stage (above the dashed line in fig. 12*b*) is a simple triode difference-amplifier. The gain of this stage can be controlled with the variable resistor R. The two stages are coupled by capacitors of 2 μF, and 2.2 MΩ grid resistors are used for the tubes in the second stage.

The total gain of the amplifiers A_1 to A_4 is approximately 5000×. The total rejection factor is approximately equal to that of the first stage and hence very high. The circuit of this amplifier stage offers

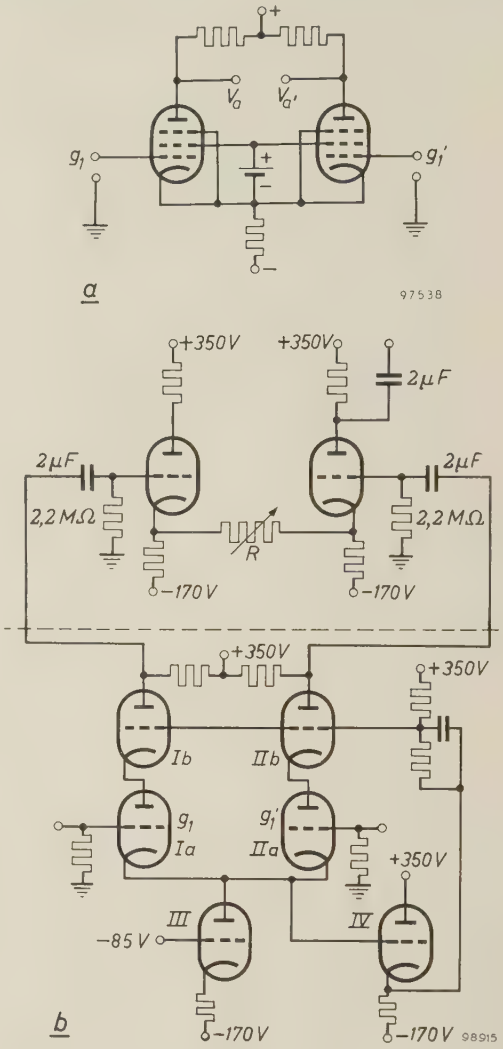

Fig. 12. *a*) Diagram of a simple pentode difference-amplifier. If both pentodes and their anode resistors are completely identical, the output signal $(V_a - V_a')$ is proportional to $(V_{g1} - V_{g1}')$ and independent of $\frac{1}{2}(V_{g1} + V_{g1}')$.
b) Circuit diagram of the pre-amplifiers (A_1-A_4 in fig. 11). The first stage (below the dashed line) can be regarded as derived from the pentode difference-amplifier (*a*), the pentodes being replaced by cascodes (i.e. the triode-pairs *Ia* and *Ib*, and *IIa* and *IIb*, connected in series), the cathode resistor being replaced by the triode *III*, and the battery supplying the screen-grid voltage by the circuit of triode *IV*. The latter circuit ensures that the grid potentials of triodes *Ib* and *IIb* closely follow the changes in the cathode potentials. This stage has a high rejection factor, although no selected tubes or resistors are employed. The second stage (above the dashed line) is a simple triode difference-amplifier, the gain of which can be controlled by the variable resistor *R*.

the very important practical advantage that the above-mentioned rejection factor is obtained without the use of specially selected tubes or resistors. Moreover, because of this very high rejection factor, no particularly high demands need be made with respect to the constancy of the supply voltage.

[6]) The impedance present between the interior of the body (which is a relatively good conductor) and an electrode plate can be represented by a resistor R and a capacitor C connected in parallel. Measurements in which the plate was applied to the body with the aid of electrode paste (this always contains an electrolyte and sometimes too an agent for softening the horny layer of the skin) and in which the skin was properly softened, showed for a plate of 9 cm²: R = 2.5 kΩ and C = 0.3 μF, and for a plate of 36 cm²: 1.5 kΩ and 0.75 μF. Less careful application of the plate made R in some cases ten times higher. The resistance of the interior of the body was found to be 260 to 270 Ω from wrist to wrist.

[7]) See G. Klein, Rejection factor of difference amplifiers, Philips Res. Repts. **10**, 241-259, 1955.

We shall give here some further details of the considerations that led to the circuit design of the first stage.

Calculations show that a difference amplifier of the type in fig. 12*a* can be given a large rejection factor by using tubes having a high amplification factor μ and by choosing the magnitude of the common cathode resistance such that the product of this resistance and the average transconductance (slope) of the tubes is of the same order of magnitude as μ. Now the effective μ value for a cascode arrangement is equal to the product of the μ values of the individual tubes, provided the grid potentials of the "upper" tubes differ by a constant amount from the cathode potentials of the "lower" tubes (and hence follow the potential changes of the latter). With such a cascode arrangement, then, a very high effective μ can be achieved. The common cathode resistance can be given a correspondingly high effective value by using a triode for this purpose, or perhaps another cascode set-up. In this way an effective value of 10 to 100 MΩ can easily be obtained. This subject is dealt with at length in the article quoted under [7]).

Mixing circuit and output amplifiers

The linear equations that express (proportionately) the components of the heart vector in terms of the potentials appearing between the electrode pairs were chosen as follows for the system with three leads (four electrodes):

$$X = \quad 8B + 54L + 16F,$$
$$Y = -\ 6B - 10L + 26F,$$
$$Z = -40B + 12L - 26F,$$

and for the system with four leads:

$$X = \quad 3B - \ 9W + 59L + 15F,$$
$$Y = -\ 2B + \ 8W - 11L + 26F,$$
$$Z = -13B + 51W - \ 2L - 27F,$$

where L, F, B and W represent the earlier-mentioned potential differences. The correct fractions of the signals from the pre-amplifiers are obtained, as we have seen, by means of potentiometer circuits. With the aid of a number of switches (on a single spindle) it is possible to switch between the coefficients of one system of equations and those of the other.

All signals having a positive coefficient in a particular equation are thereupon fed to an adding circuit; those having a negative coefficient likewise. These adding circuits are equipped with triode cathode followers (three at most) and with a common anode resistance (*fig. 13a*). Since a single projection calls for no more than two summations at a time, only four such adding circuits are required. (One circuit in each pair contains a triode whose control grid is maintained at earth potential and whose cathode resistance is variable (fig. 13*b*); this makes it possible to shift the patterns on the oscilloscope screen.) Of each pair of adding circuits, then, one supplies the absolute value of the sum of the positive terms, and the other that of the sum of the negative terms of the equation concerned. A signal proportional to the difference of both sums

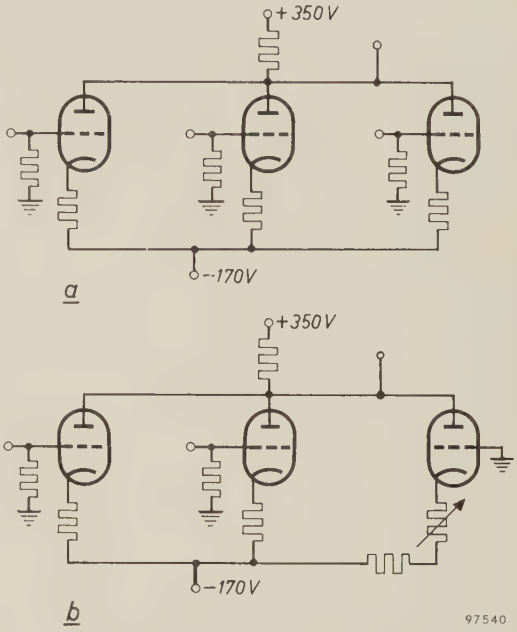

Fig. 13. *a*) Adding circuit with three triodes connected in parallel, with a common anode resistor and identical cathode resistors. The signals to be added are applied to the three grids; the sum signal is proportional to the variations of the anode voltage. *b*) Similar circuit in which one triode has an earthed grid and a variable cathode resistor. By means of this triode a constant voltage can be applied to the sum signal, making it possible to change the position of the pattern on the oscilloscope screen without affecting the shape of the oscillogram.

is obtained by applying the summed signals to one of the output amplifiers. These are again designed as difference amplifiers (*fig. 14*). The amplification of the difference signal (max. 60×) can be reduced continuously by approximately a factor of 10. A large rejection factor is not necessary here.

The frequency response of the whole apparatus is determined at the low-frequency side by that of the pre-amplifiers together with the mixing circuit, and at the high-frequency side by that of the output amplifiers. The lower limit of the frequency band passed by the apparatus is mainly determined by the value of the capacitor that couples the pre-amplifier to the potentiometers in the mixing circuit, and by the resistance of these potentiometers (2 μF and 1.2 MΩ, respectively). The coupling between the two pre-amplifier stages has an even higher RC value (2 μF × 2.2 MΩ) and is of secondary significance. The frequency at which the gain has dropped to 70% ($1/\sqrt{2}$) is approximately 1/12 c/s. The upper limit of the frequency band is approximately 100 c/s. The choice of this upper limit is determined partly by the consideration that a

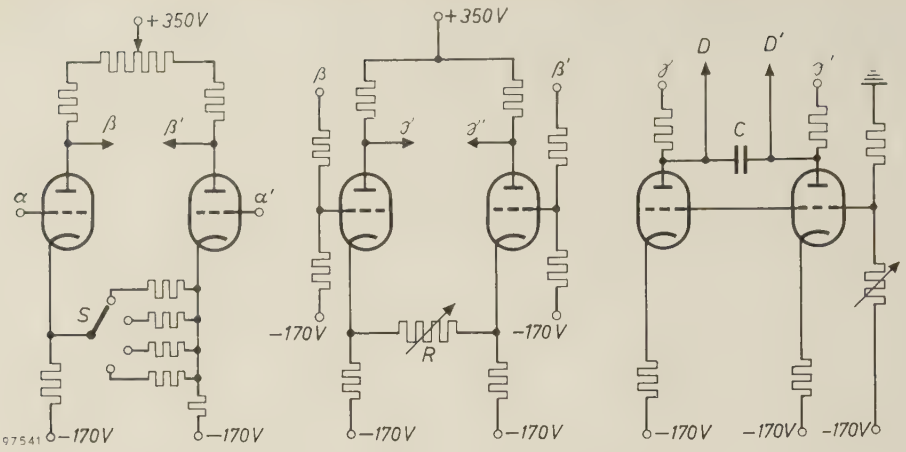

Fig. 14. Circuit diagram of output amplifiers. The first stage (left) is connected to the second stage (centre) at the positions β and β', the second stage to the output stage (right) at the positions γ and γ'. Both stages are difference amplifiers. The input terminals of the first stage are the points a and a'. The gain can be varied in four steps by switch S (approximately as 1:2:4:8) and continuously with the variable resistor R. The function of the output circuit is to enable the output signal of the second stage, appearing at (γ, γ') where the average potential is about +230 V, to be applied without any attenuation to the deflection plates D, D', where the average potential is that of earth. The capacitor C together with the resistors of the output circuit determines the upper limit of the frequency band passed by the amplifiers.

higher limiting frequency is unnecessary for cardiography, and partly by the fact that a higher value would increase the influence of interfering potentials from other muscles.

Beam modulator

The beam modulator consists, as mentioned, of three parts: one which periodically suppresses the beam, one for varying the intensity with the writing speed, and one which enables the projection to be only partly displayed. The latter two parts have one section in common. A diagram of the whole modulating system is given in *fig. 15*. The common section referred to is found in (A) above the upper dashed line. It consists of two double triodes connected in parallel and each with a common cathode. The grids of each double triode are connected via coupling capacitors of 1500 pF to the ends of the output amplifiers, that is to say each grid is connected to one of the four deflection plates of the oscilloscope. Since the changes in the potential on the plates of one pair are always equal but opposite, this also applies to the signals fed to the grids of the relevant pair of triodes. The latter signals are approximately proportional to the time derivatives of the potentials on the deflection plates, i.e. they are approximately proportional to the horizontal and vertical components, respectively, of the writing velocity of the spot on the oscilloscope screen. The negative signal from each pair rapidly cuts off the relevant triode, whilst the positive signal determines the current through the common cathode resistor. The output signal from this part of the circuit is therefore approximately proportional to the sum of the absolute values of the horizontal and vertical velocity components of the spot on the screen, and thus varies in approximately the same way as this velocity. Through the circuit in B this signal, which is always positive, is fed to the output (g_1, in D), i.e. to the control grid of the cathode-ray tube. The intensity of the electron beam is consequently higher when the writing velocity is greater, so that the line traced has roughly uniform thickness.

Also connected directly to the output is the circuit shown in C. This is simply a multivibrator, whose function is to interrupt the electron beam periodically and thus to provide the time marking. If the switch S_1 is in position N, the multivibrator is out of operation, and an uninterrupted trace is obtained. In the other case the beam is interrupted 200 times per second.

The third function of the beam modulator, which is to suppress the beam during a certain part of the cardiac cycle, is performed by the circuit shown in E and F. F contains two monostable multivibrators [8]) with variable pulse width. The pulse width of the one on the right governs the length of the time interval during which the electron beam is passed or

[8]) A monostable multivibrator has one stable and one quasi-stable state. A trigger pulse of the appropriate sign drives the circuit into a state in which the tube that was conductive is cut off and the other made conductive; after a predetermined period the circuit returns to the original state. The output signal is a rectangular voltage pulse whose duration is equal to the above predetermined period.

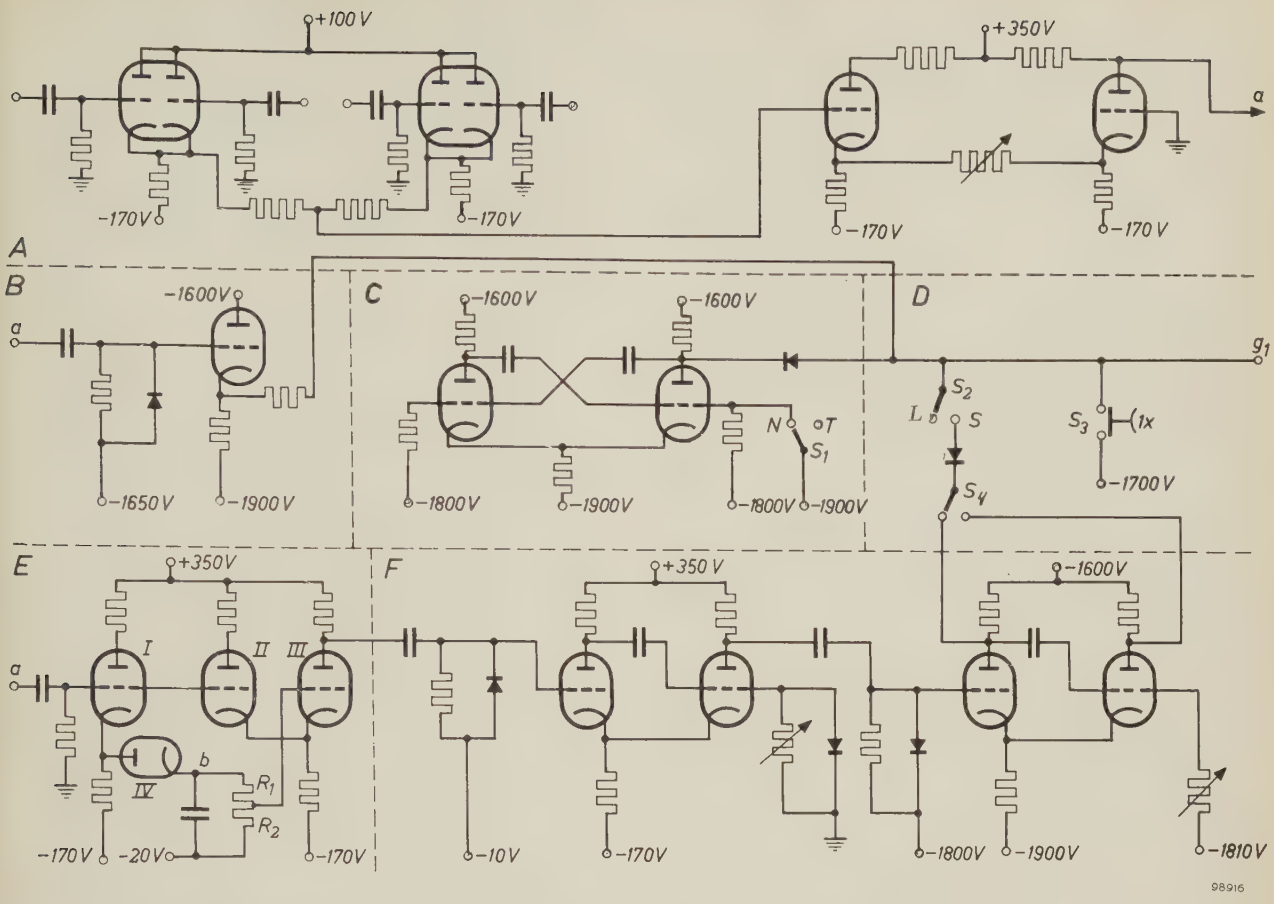

Fig. 15. Circuit diagram of beam modulator which *a*) makes the thickness of the beam vary with the writing speed, *b*) enables a certain part of the figure to be suppressed, and *c*) periodically interrupts the beam. The circuits fulfilling the first two functions have a common section (*A*), the signal from which is approximately proportional to the sum of the absolute values of the horizontal and vertical components of the writing speed (i.e. proportional to the sum of the derivatives — obtained via the coupling capacitors — of the potentials of the positive plate of each pair of deflection plates). This signal is amplified by the two triodes shown on the right of section *A*, and serves as the input signal for section *B* and also for section *E*. The first simply applies the signal to the output of the beam modulator (g_1, section *D*), i.e. to the control grid of the cathode-ray tube. The purpose of the diode (section *B*) is to prevent the triode grid potential from falling below the quiescent value. This circuit performs the function mentioned under *a*). The circuit in section *E* delivers a trigger pulse once per heart beat to the first monostable multivibrator [8]) in section *F*, exactly at the moment at which the incoming signal has maximum amplitude. The operating period of both monostable multivibrators (*F*) is variable. The period (pulse width) of the second determines the length of time the beam shall be suppressed (or passed, depending on the position of S_4), whilst that of the first monostable multivibrator determines the moment at which this time interval begins. Switch S_2 makes and breaks the connection with the output. The circuit in section *C*, a multivibrator, supplies the square-wave voltage for periodically interrupting the electron beam (function *c*). The multivibrator oscillates when S_1 is in position *T*. The diodes in sections *C* and *D* break the connection with g_1 as soon as the potential at the output of the circuit concerned rises above that produced by section *B* on g_1. S_3 is a push-button for manually suppressing the beam.

suppressed (depending on the position of switch S_4). The pulse width of the other governs the moment at which this time interval begins. During each cardiac cycle this monostable multivibrator is triggered at corresponding moments by the circuit shown in *E*. The signal applied to this circuit is the output signal from the circuit in branch *A*, and is thus proportional to the sum of the absolute values of the two velocity components of the light spot. For each heart beat this signal consists of a number of peaks, which are always positive and one of which is usually considerably larger than the others. This large peak, the top of which coincides with the moment at which the writing velocity in the *QRS* loop is at maximum, makes the diode *IV* conductive, thus increasing the potential on point *b*, and hence also (to an extent determined by potentiometer R_1-R_2) the potential on the grid of triode *III*. As a result triode *III* passes a fairly high current and triode *II* is cut off. Owing to the very high *RC* constant of the circuit in question (3.5 sec) this situation is maintained long enough to prevent the diode *IV* or the triode *II* from being made conductive by any of the smaller peaks following upon the maximum peak during the same heart beat, or by those preceding this peak during the following heart beat. Only the large peak of the successive heart beat can make these tubes conductive, and thus only at the moment of its arrival does the circuit deliver a trigger pulse to the first monostable multivibrator in *F*.

Other circuits

Finally, some remarks about the power-supply circuits, the cathode-ray tube and the calibrating oscillator. As regards the first of the two supply circuits it need only be mentioned that its output voltage is 520 V, the potential of one terminal being —170 V and that of the other +350 V. The output voltage (520 V) and the potential on the negative terminal (—170 V) are stabilized. A 10% mains fluctuation changes the output voltage by approx. 50 mV and the potential on the negative terminal only by about 3 mV. This circuit supplies not only the anode voltage for the various components of the vectorcardiograph, but also the filament current for the pre-amplifier tubes and for various tubes in the supply circuits. For this purpose the filaments of these tubes (all type UCC 85; heater current 100 mA) are connected in series.

The other supply circuit, which among other things provides the high tension for the cathode-ray tube, is shown in *fig. 16*. Here again, use is made of the properties of series-connected triodes. This circuit, details of which are given in the subscript to the figure, can only be employed, however, in

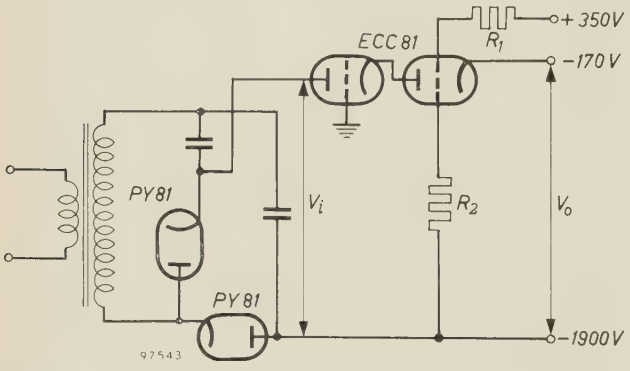

Fig. 16. Simplified diagram of the circuit that supplies the stabilized direct voltage for the cathode-ray tube and for certain components of the beam modulator. The output voltage V_o is very well stabilized with respect to variations in V_i (i.e. the mains voltage), but less so with respect to load variations. The proportionality factor between the variations in V_i and V_o for this circuit is $\mu R_1/(R_1+R_2)$, where μ is the effective amplification factor of the cascode. Since $\mu = 3600$ and $R_1/(R_1+R_2) = \frac{1}{4}$, this factor is 900. The stabilized voltage for the cascode grids is supplied by the other power-supply circuit of the vectorcardiograph (+350 V, —170 V). The voltage V_i is obtained from a high-tension transformer (secondary voltage approximately 800 $V_{r.m.s.}$) and a voltage-doubling rectifier circuit.

applications where the current drain is low and fairly constant.

The cathode-ray tube is of the type DP 13-2 with both blue and yellowish-green fluorescence. The blue component has a short afterglow, which is an advantage when photographing the screen, and the yellowish-green component has a long afterglow, which is an advantage for visual observation.

The calibration-voltage generator delivers a sinusoidal signal of variable amplitude (max. 1 $V_{r.m.s.}$ approx.) and 25 c/s frequency. With the voltage output from this oscillator it is possible to check not only the operation of the amplifiers (for both gain and rejection factor) but also all connecting leads, including the lead used for earthing the patient (see below).

Suppressing of external interference

The chief form of external interference experienced in cardiography is induction from the electric mains (hum). In the first place this causes the potential of the body as a whole to fluctuate, and secondly it gives rise to potential differences between the various points on the surface of the body. The average potential difference between the body and earth can be reduced to a few mV at the most by earthing the patient. (We have in mind a patient in a normally equipped laboratory or hospital ward, but not of course a case where the patient is very close to cables carrying the mains voltage.) The limiting factor here is the resistance of the skin which, as mentioned earlier, can amount to several kΩ. In the apparatus described the patient is earthed via the right leg. Owing to the high rejection factor of the pre-amplifiers, the hum signal after earthing is not troublesome. The potential difference induced between the various parts of the body is found to be 20 to 30 μV between the wrists of the left and right arm when the patient is earthed via the right leg. This is just below the nuisance limit, and therefore it is possible with this apparatus to record vectorcardiograms at any required location without special precautions being necessary.

The influence of a second kind of external interference, namely microphony caused by mechanical vibrations, is eliminated by spring-suspension of the pre-amplifiers.

Practical significance of vectorcardiography

Although vectorcardiography is still to some extent in the stage of research and is not yet in general clinical use, it has already proved its great practical value as a method of examining the heart.

A very useful property of the vectorcardiogram is that its shape can fairly easily be correlated with the anatomy of the human heart. This means that it is comparatively simple to learn to interpret a vectorcardiogram, whereas for interpreting the results of a conventional electrocardiographic examination it is necessary to memorize a large number of patterns whose relation to the anatomy of the heart is by no

means obvious. Experience has shown that a physician who has first practised vectorcardiography and then proceeds to study ordinary electrocardiography is able to grasp this relationship more readily and thus to interpret conventional electrocardiograms accurately sooner than others; there is thus no doubt that vectorcardiography also possesses didactic value. In some pathological cases the electrical phenomenon is so capricious as to defy interpretation by the conventional electrocardiographic method. In such cases the vectorcardiogram may often provide the answer. Certain details appearing in the vectorcardiogram are often not sufficiently evident in a conventional electrocardiogram to be detected.

In connection with simplicity of interpretation, moreover, it may be added that it is easier to interpret shapes than to read graphs.

An important particular that can be directly deduced from a vectorcardiogram is the sense of rotation of the heart vector. True, this can also be derived from ordinary electrocardiograms, but only by ascertaining the moment at which corresponding peaks occur in the various leads (cf. fig. 9).

Because of the ease of interpretation it offers and the reasonably high percentage of cases in which the heart vector is recorded with good accuracy, vectorcardiography in its present form can already be used as a routine screening test and is in fact so used in Eindhoven. It offers the physician the possibility of rapidly determining the location and the nature of a disorder.

Since vectorcardiography looks at the heart, as it were, from a distance and provides no information on an individual small part of the heart, it is not to be expected that it will ever entirely supersede conventional electrocardiography, which can provide detail information. The one method will supplement the other, in the sense that conventional electrocardiography will continue to provide additional detailed information.

Summary. The electrical action of a contracting muscle fibre is equivalent to that of a dipole and can be represented by a vector. The same applies to an entire muscle, such as the heart, insofar as the electrical phenomena are observed at a large distance from the source. During the heart beat the heart vector changes in magnitude and direction. Since the human body is a conductor, the electrical action of the heart manifests itself in the form of potential differences between various points on the surface of the body; these potential differences show marked variations as a function of time, and recorded they produce the conventional electrocardiogram. By applying electrodes to at least four positions on the body and combining the independent potential differences in the correct manner — the relation between the components of the heart vector and each of these potential differences is a linear one — the 3-dimensional curve can be found that represents the variation of the heart vector with time (called the vector-electrocardiogram). In the vector-electrocardiograph described, two of the three mutually perpendicular components of the heart vector are "computed" from the potential differences mentioned and proportional voltages are applied to the horizontal and vertical deflection plates of a cathode-ray oscilloscope. Successive recordings are thus made of the frontal, horizontal and sagittal projections of the vectorcardiogram. Time marks are obtained by periodically interrupting the electron beam; the sense of rotation of the curve is found by breaking off the recording at a certain moment. The use of difference amplifiers having a high rejection factor makes the apparatus very insensitive to external interference that causes equal fluctuations of the electrode potentials (hum). Since the form of vectorcardiograms can be fairly simply correlated with the anatomy of the heart, it is easy to learn to interpret them. Even in its present form vectorcardiography can already be put to good use for didactic purposes and as a routine screening test. Moreover the significance of some details in a conventional electrocardiogram sometimes only becomes clear after comparison with a vectorcardiogram. The nature of the method justifies the conclusion that vectorcardiography will prove a useful supplement to conventional electrocardiography, but will not supersede it.

ABSTRACTS OF RECENT SCIENTIFIC PUBLICATIONS BY THE STAFF OF N.V. PHILIPS' GLOEILAMPENFABRIEKEN

Reprints of these papers not marked with an asterisk * can be obtained free of charge upon application to Philips Electrical Ltd., Century House, Shaftesbury Avenue, London W.C. 2.

2638: H. G. van Bueren: Versterkers voor licht en radiostraling uit de wereldruimte (Ned. T. Natuurk. **24**, 189-205 and 213-228, 1958, Nos. 8 and 9). (Amplifiers for light and radio waves from space; in Dutch.)

Survey of a number of modern detectors of light and microwaves for use in experimental astronomy. While "classical" light detectors such as the photographic plate and the photocell have adequate *absolute* sensitivity, it is nevertheless worth while to investigate any methods which might shorten observation times or improve resolution, particularly for large faint objects or objects whose brightness varies rapidly. Radio waves from outer space are very weak and have the character of noise; their detection and investigation requires receivers of very low noise level. Modern developments in microwave techniques and solid state physics have led to totally new approaches to the amplification of radiation. Among the new devices discussed here are masers, parametric amplifiers and various types of light amplifiers.

2639: J. Davidse: Versuche über die Anpassung des NTSC-Farbfernsehsystems an die europäische 625-Zeilen-Norm (Nachr.tech. Z. **11**, 461-466, 1958, No. 9). (Investigation of the application of the N.T.S.C. colour-television system to the European 625-line standard; in German.)

Investigations into the factors which determine system parameters of transmission systems for colour television according to the American N.T.S.C. system. The work is particularly directed to the application of the N.T.S.C. system to the 625-line television standard (Gerber-standard) used in certain countries on the continent of Europe. The choice of the two colour signals and their bandwidths and the choice of the sub-carrier frequency are discussed. Experiments on loss of sharpness as a result of bandwidth restriction of the colour information and on crosstalk phenomena show that the optimum choice of the system parameters is primarily governed by the statistical properties of the colour signal.

R 364: K. F. Niessen: Distribution of magnetic domains between the two phases in a single-crystal flat disk of iron (Philips Res. Repts. **14**, 101-110, 1959, No. 2).

A single-crystal oblate spheroid of iron is considered whose plane is a (001) plane of the crystal. It is subjected to a magnetic field H lying in the first quadrant of this plane, making an angle with the second of the two preferential axes [100], [010] which lie also in the plane. The total number of magnetic domains is called N, all being of the same moment m, whereas Nm is supposed to be known. The ratio in which these domains are distributed between the preferential directions of the crystal depends on the strength H of the external field. The graphical determination of this ratio is the aim of the present paper. It is compared with the analytical determination given by Néel and by Lawton and Stewart.

R 365: K. Böke, J. B. M. Spaapen and N. B. Speyer: Diffusion capacitance in transistors (Philips Res. Repts. **14**, 111-122, 1959, No. 2).

Capacitance measurements have been performed with transistors at different temperatures, voltages and frequencies. Calculations of the diffusion capacitance (= injection or storage capacitance) have been carried out, taking into account the influence of the second junction. Theory and experiment both indicate that this influence can be very large. The calculations are in qualitative and quantitative agreement with the measurements.

R 366: W. Ch. van Geel and C. A. Pistorius: Current-time relationship in the forward direction of electrolytic rectifiers (Philips Res. Repts. **14**, 123-131, 1959, No. 2).

The shape of the forward current as a function of time is given for an electrolytic rectifier, if an alternating rectangular voltage is applied. The loops in the current-voltage characteristic, which occur when a sinusoidal voltage is applied, are explained. It appears that the forward current decreases strongly with increasing blocking voltage.

The forward current through the oxide layer hardly depends on the thickness of this layer. A qualitative explanation of the observed phenomena is given.

R 367: G. Brouwer: Three-dimensional electric-circuit model of the high-frequency phenomena in a junction transistor (Philips Res. Repts. **14**, 132-142, 1959, No. 2).

In order to give a complete explanation of the high-frequency behaviour of a junction transistor both minority- and majority-carrier flow must be taken into account. Owing to the large number of complicated boundary conditions, it is not possible to give the solution in a closed mathematical form. The linearized problem, corresponding to small-signal operation of the transistor, may be solved with the aid of an electric-circuit model. The high-frequency current gain of the transistor may be derived from model experiments.

R 368: J. J. Scheer and P. Zalm: Crystal structure of sodium-potassium antimonide (Na_2KSb) (Philips Res. Repts. **14**, 143-150, 1959, No. 2).

X-ray analysis of Na_2KSb — a photoemissive material discovered by Sommer — has led to the determination of its crystal structure. The unit cell is described by the space group $Fm3m\text{-}O_h^5$ with four antimony atoms at $(0,0,0;\ 0,\frac{1}{2},\frac{1}{2};\ \frac{1}{2},0,\frac{1}{2};\ \frac{1}{2},\frac{1}{2},0) + 0,0,0$; four potassium atoms at $(\quad) + \frac{1}{2},\frac{1}{2},\frac{1}{2}$ and eight sodium atoms at $(\quad) + \frac{1}{4},\frac{1}{4},\frac{1}{4}$ and $\frac{3}{4},\frac{3}{4},\frac{3}{4}$. The crystal structure of Na_2KSb has a great resemblance to that of Cs_3Sb and differs strongly from that of Na_3Sb and K_3Sb which both crystallize in the Na_3As type.

R 369: N. C. de Troye: Classification and minimization of switching functions (Philips Res. Repts. **14**, 151-193, 1959, No. 2).

Electronic computers consist of a large number of switching elements, of which there are relatively few types, which together are capable of handling or forming a large number of conditions. A special switching technique, with the aid of diodes, is now being used for those parts of the machine where extremely short switching times are required. For several reasons it is advisable to keep the number of diodes as small as possible. To study the various conditions to be realized with diode circuits, Boolean algebra may be profitably applied. It may be demonstrated that two forms of notation in Boolean algebra, viz. the minimal sum of products and the minimal product of sums, are of particular importance in diode-circuit configurations. Several authors have attempted to arrive at these two forms of notation with varying degrees of success. This paper (thesis, Amsterdam 1958), too, is an attempt to find from a given Boolean function — also called switching function in view of its application in computer techniques — either the minimal sum of products or the minimal product of sums. It is demonstrated that it is possible to transform any given switching function into a matrix containing only the elements 0 or 1. The number of elements 1 in the various submatrices indicates whether a simplified notation of the switching function is possible. The possibility of easily finding the prime implicants of the switching function is likewise shown. These prime implicants can then be used to determine the minimum sum of products. It is found that this process can be carried out by means of electronic computers. The number of switching functions of n variables is 2^{2^n}. As is demonstrated, it is not necessary to determine the minimum sum of products for all these switching functions if the concept of equivalence class (i.e. the set of all switching functions that are invariant as regards permutation and negation of variables) is introduced. Every equivalence class has a representative and it is only of this representative that the minimal sum of products has to be obtained. Determining the equivalence class for any given switching function of 3 or 4 variables is a relatively simple matter.

R 370: W. L. Wanmaker, M. L. Verheijke and W. Parchen: Influence of the "dope" on the reduction rate of tungsten trioxide by hydrogen (Philips Res. Repts. **14**, 201-206, 1959, No. 3).

The influence of water vapour, layer thickness and presence of additives ("dopes"), e.g. K silicate and $K_4SiW_{12}O_{40}$, on the reduction rate of WO_3 is studied. K silicate and $K_4SiW_{12}O_{40}$ increase the reduction rate, but only if thick layers of WO_3 are reduced. The presence of water vapour imparts a retarding action to the reduction, which is less pronounced with the doped products.

R 371: H. U. Harten: Influence of the ambient atmosphere on the surface recombination of silicon (Philips Res. Repts. **14**, 207-210, 1959, No. 3).

From measurements of the surface photo-voltage it follows that the surface potential of silicon can be altered, similarly to that of germanium, over a wide range by chemical surface treatments and over a smaller range by the ambient atmosphere. Simultaneous investigation of the surface recombination

shows this process to be determined chiefly by recombination centres of the "Hall-Shockley-Read" type.

R 372: M. Avinor: Edge photoconductivity of cadmium sulphide (Philips Res. Repts. **14**, 211-214, 1959, No. 3).

It is shown that the characteristic photoconductivity peak of single crystals of cadmium sulphide at 515 mμ is not due to band-band transition. An additional photoconductivity peak is observed at 500 mμ by activation with silver in excess of co-activator. Superlinearity at room temperature was also observed.

R 373: Nathan Spielberg: Intensities of radiation from X-ray tubes and the excitation of fluorescence X-rays (Philips Res. Repts. **14**, 215-236, 1959, No. 3).

The intensity of fluorescence X-rays is discussed in terms of the efficiency of conversion of given primary wavelengths to fluorescence radiation and the spectral distribution of the primary radiation from the X-ray tube. For single-element specimens and major constituents of multiple-element specimens in the geometries normally used in modern spectrochemical analysis, the conversion efficiency varies slowly with primary wavelength if the exciting wavelength is not too far from the specimen absorption edge. In these cases the fluorescence intensity is affected primarily by the radiation flux, expressed in photons/second, from the exciting X-ray tube, and not so much by its wavelength distribution. For minor constituents of the specimen and/or when the exciting radiation is far from the specimen absorption edge, the conversion efficiency varies with the cube of the primary wavelength. The expected spectral intensity distribution, both in the characteristic and the continuous spectrum, from an X-ray tube target is discussed as a function of the target material. For the X-ray spectrochemical analysis of light elements (lighter than sulphur), the *L*-series radiation from a Mo or Ag target tube may lead to a large increase in fluorescence intensity. Experimental results confirming certain aspects of the theory are presented, and the need for further experiments, particularly with respect to soft X-rays, is pointed out.

R 374: J. Hornstra and P. Penning: Birefringence due to residual stress in silicon (Philips Res. Repts. **14**, 237-249, 1959, No. 3).

Rapid cooling of large silicon crystals gives rise to plastic deformation, as can be deduced from the increase of the etch-pit density. Additional information is obtained from a study of the residual stress by observation of the birefringence with infrared light. When slices are cut from the quenched cylindrical crystal the stresses change. The calculated stresses are corrected for this effect. Tensile stress is measured by compensation with external pressure. Also the optical phase difference is determined and, by comparison of the two, the stress-optical constant. The authors found a smaller value than Giardini; the difference, however, need not be significant. The experiments strongly suggest that a very large part of the thermal stress is released by plastic deformation, when the initial temperature is above 1300 °C. Residual stresses are also found in bars that have been bent at 750 °C. From the stress pattern the stress distribution during plastic flow can be derived. This gives directly the relation between flow rate and stress. In some cases the relation $\dot{\varepsilon} \propto \sinh(\sigma/\sigma_0)$, introduced by Van Bueren, was found; but often the stress pattern was more complicated due to the beginning of work hardening.

R 375: N. C. de Troye: Classification and minimization of switching functions (Philips Res. Repts. **14**, 250-292, 1959, No. 3).

Continuation of **R 369**.